

Laser and IPL Technology in Dermatology and Aesthetic Medicine

Christian Raulin
Syrus Karsai
Editors

Laser and IPL Technology in Dermatology and Aesthetic Medicine

Christian Raulin • Syrus Karsai
(Editors)

Laser and IPL Technology in Dermatology and Aesthetic Medicine

 Springer

Editors

Prof. Dr. Christian Raulin
Laserklinik Karlsruhe
Kaiserstr. 104
76133 Karlsruhe
Germany
info@raulin.de

Dr. Syrus Karsai
Laserklinik Karlsruhe
Kaiserstr. 104
76133 Karlsruhe
Germany
info@raulin.de

ISBN 978-3-642-03437-4 e-ISBN 978-3-642-03438-1
DOI 10.1007/978-3-642-03438-1
Springer Heidelberg Dordrecht London New York

Library of Congress Control Number: 2010937978

© Springer-Verlag Berlin Heidelberg 2011

This work is subject to copyright. All rights are reserved, whether the whole or part of the material is concerned, specifically the rights of translation, reprinting, reuse of illustrations, recitation, broadcasting, reproduction on microfilm or in any other way, and storage in data banks. Duplication of this publication or parts thereof is permitted only under the provisions of the German Copyright Law of September 9, 1965, in its current version, and permission for use must always be obtained from Springer. Violations are liable to prosecution under the German Copyright Law.

The use of general descriptive names, registered names, trademarks, etc. in this publication does not imply, even in the absence of a specific statement, that such names are exempt from the relevant protective laws and regulations and therefore free for general use.

Product liability: The publishers cannot guarantee the accuracy of any information about dosage and application contained in this book. In every individual case the user must check such information by consulting the relevant literature.

Cover design: eStudioCalamar, Figueres/Berlin

Printed on acid-free paper

Springer is part of Springer Science+Business Media (www.springer.com)

Foreword I

At the publication of this volume, lasers are half a century old, or perhaps it is more accurate to write half a century young. The interplay between light and matter fascinated Albert Einstein, whose $E=mc^2$ expresses the fact that all matter and all energy are equated by only one constant – the speed of light. He also figured out that the only “thing” different observers measure as being constant – is the speed of light. Apparently, we live in a universe not only bathed in light, but defined by it. Einstein’s work on quantum electromagnetism is less well-known, but anyone using a laser should appreciate that the device exists because of it. Fundamentally, creation of a photon is the time-inverse of its absorption. In an excited atom, it is possible for photons to stimulate the creation of more photons. Stimulated emission, the S.E. of L.A.S.E.R., is at the heart of every laser. Charles Townes and colleagues made the first device using stimulated emission to amplify (the “A” in L.A.S.E.R.) microwave photons, and in a few years this was done with light (the “L” in L.A.S.E.R.).

Is an understanding of laser operation important to a physician using a laser? Yes! Extreme power, coherence, well-defined wavelength, ability to generate very brief pulses, and to focus tightly, are all properties of lasers important to their medical applications. In dermatology, we use lasers mainly as surgical tools to heat or vaporize cells and tissue with precision and often with selectivity, i.e., preferentially affecting some light-absorbing targets within the skin. This excellent book is a thorough and practical description of those applications, which depend on high-power pulses at well-defined wavelength regions. Sometimes, a xenon flashlamp can be used for selective photothermolysis of large targets such as hair follicles or blood vessels. The selectivity possible with flashlamps is always inferior to that possible with lasers, but in practice, is often sufficient. For very small targets such as the isolated dermal melanocytes of nevus of Ota, or tattoo ink-containing cells, very powerful short pulses are needed to achieve safety and efficacy. Lasers are the only sources able to deliver such pulses.

In other applications, such as fractional photothermolysis, it is necessary to deliver light in a microbeam, or as an array of small foci. Again, lasers are ideal for this application. Fractional laser treatments at present are not selective for some specific target in the skin. However, we can expect that “smart” laser microbeam treatments will be developed that will use imaging to identify which tissue structures the laser should expose. These devices may create another paradigm for laser dermatology, because some of the most important target structures in skin are not pigmented.

The coherence property of lasers is not used much in dermatology, but it will be. Coherence can be thought of as a measure of how much alike photons in a beam are, with respect to each other. High coherence lasers are used to make holograms, and in

medicine to measure blood flow by laser doppler velocimetry. Lasers have revolutionized biological microscopy for research. They will probably revolutionize microscopy of living skin, with further development. A combination of high brightness and low coherence offers the potential for deep, high-speed microscopy of skin. Optical coherence tomography and related approaches used widely in ophthalmology, are entering cardiovascular and endoscopic imaging applications, and have strong potential in dermatology.

Ultimately, it is clinical practice that defines the therapeutic and diagnostic use of lasers. As such, clinical dermatologists have a major role to play in motivating the creation of new applications and new medical lasers. This book offers practical knowledge, practical uses, and a thorough understanding of the risks and benefits posed by a wide spectrum of medical lasers and related technologies.

People are not pastries. If you treat them according to a fixed recipe, they will sometimes be overcooked. The natural variations of skin structure, pigmentation, sun exposure, wound healing, age, and gender are important for not only laser dosimetry, but also for the fundamental decisions of whether to treat and if so, with which device(s). These are also the natural variations that make medicine an art, as well as a science. Enjoy!

Boston, MA, USA

Prof. Dr. R. Rox Anderson

Foreword II

When amplified by stimulated emission of radiation, light may have unique properties capable of causing novel reactions in biological materials. In complex multicellular organisms, the host responses to this form of electromagnetic radiation may also be unique resulting in outcomes different from those expected from traditionally described response to injury.

Until the twentieth century, the complex forces guiding the evolution of human responses to injury were never influenced by the collective properties of lasers or IPL technology. By altering the properties of lasers, savvy investigators have explored the creation of selective tissue injury with novel combinations of spatial localization and mechanisms of tissue alteration. The form of injury may be manipulated to stimulate a cascade of repair responses aimed at correcting a variety of lesions in skin and other organs. The precision of tissue alteration can not be achieved by other means. This book contains many examples – written by those who discovered the response pathway and those who have successfully exploited the tissue response to develop and constantly improve the diagnostic and therapeutic use of lasers and IPL technologies.

We expect more rapid growth of the technologies that creates unique energy waves, pulses, and “packets” of energy. We expect advances in molecular biology, pathology, optical diagnostics, and molecular tagging to lead a better understanding of tissue response to radiation. We expect investigators versed in biology, photochemistry, nanotechnology, electronics, and photophysics to continue the rapid development of this technology in subsequent medical and surgical uses.

There will always be those creative investigators who understand both the technical and biological parameters enough to capture selected portions of tissue responses at the right place at the right time in the right organ.

This book may be viewed as an update in the impression progress made to date and a foundation for future advances.

Boston, MA, USA

Prof. Dr. John A. Parrish

Preface

Laser and IPL technology have brought about thorough ongoing changes in the treatment options for many clinical pictures encountered in dermatology during recent years. The specialism of aesthetic medicine has benefited greatly from all this. The rapid technical progress and the frequent emergence of new equipment and indications make it extraordinarily difficult for the interested doctor to get an overview of the research position and the possibilities and the limitations of these procedures. Disconcertingly, popular science publications also have a role in all this, so that the need for factual and objective information is constantly becoming more intense, especially as there are very few evidence-based scientific studies available on the possible applications of new laser techniques. In addition, the time elapsing between current knowledge and developments and their practical implementation is becoming shorter and shorter.

This book is addressed equally to specialists who already have experience in using laser and IPL systems and to doctors and students who harbor the ambition of becoming well-informed about the specific treatment options so as to be in a position to give patients competent advice. Without a precise and structured digest of results from research and technology, including the most recent, it is not possible for the clinician to guarantee up-to-date and correct care of the patient.

We have been able to secure international opinion of leaders for all the chapters of this book. This was the only way to fulfill our own ambition of taking full account of the rapid further development of the specialist area and to give the reader an up-to-date overview of laser therapy in dermatological-aesthetic medicine and its fringe areas, including photodynamic therapy. We have tried consistently to achieve a uniform presentation, with reference also to terminology and the structure of the texts. Where there turned out to be differences in various authors' opinions, both sides had the chance to make their case.

This textbook gives the theoretical bases of laser and IPL technology and reviews the voluminous current knowledge on the various indications. References to unsolved problems or questions that are still under discussion are found in the appropriate text sections. The chapters each have a list of the background literature and further reading matter. It would not have been possible to avoid overlappings and repeats, and they are intentional to ensure that each of the individual texts can be complete in itself.

We are particularly concerned to profile conventional alternatives to laser treatment insofar as they are better based in medicine and more economical. The quality of a method is determined to a decisive degree by careful observation of indications, and laser and IPL technology are far from being a universal panacea – not least because of the potential risks inherent in them. We therefore thought it was important

to sensitize the reader to complications, safety, administration of treatment by persons with no medical qualifications, and forensic considerations.

This book is no more able than any other to be a substitute for first-hand experience with patients. Consultation and critical analysis of diagnosis and therapy options remain an essential component of the doctor's work. For this reason one chapter is devoted entirely to ethical aspects of laser therapy.

Our sincere thanks are due to all the authors for their committed cooperation on this multiauthor work. We thank our staff assistants and colleagues for their constructive criticisms and their many hours of hard work without which it would not have been possible to prepare the book within the planned time frame. All patients who are recognizable in the illustrations have kindly given their consent to this. At this point, we should like to thank them cordially for their support. Our book is not made up solely of theory, but takes life from the many illustrative clinical examples. Not least, we are very grateful to Springer-Verlag, especially the clinical medicine editors Dr Tobias Kemme, Dr Sverre Klemp and Mrs Ellen Blasig, for their efficient project management and the successful structure of the book, and Mr Sreejith Viswanathan for his excellent editorial work.

We are pleased to say we feel confident that this text has presented laser and IPL therapy as used in dermatology and aesthetic medicine in a well-rounded manner and on the basis of comprehensive and up-to-date knowledge of the current scientific status.

Karlsruhe, autumn 2010
Karlsruhe, autumn 2010

Prof. Dr. Christian Raulin
Dr. Syrus Karsai

Contents

Part I Basics

- | | |
|--|----|
| 1 Basic Laser Physics | 3 |
| Rudolf Steiner | |
| 2 Laser-Tissue Interactions | 23 |
| Rudolf Steiner | |
| 3 Intense Pulsed Light Technology | 37 |
| Karin Kunzi-Rapp and Rudolf Steiner | |

Part II Indications

- | | |
|--|-----|
| 4 Benign Tumors and Organoid Nevi | 43 |
| Stefan Hammes | |
| 5 Facial Rejuvenation and Other Clinical Applications
of Intense Pulsed Light | 61 |
| Peter Bjerring and Kaare Christiansen | |
| 6 Inflammatory Dermatoses: Acne | 83 |
| Mathew W. Ludgate and Jeffrey S. Orringer | |
| 7 Inflammatory Dermatoses: Other than Acne Vulgaris | 95 |
| Pablo Boixeda, Lorea Bagazgoitia, João Borges da Costa,
and Maria Calvo | |
| 8 Laser-Assisted Liposuction | 113 |
| Boris Sommer and Dorothee Bergfeld | |
| 9 Photoepilation of Unwanted Hair Growth | 125 |
| Annesofie Faurschou and Merete Haedersdal | |
| 10 Pigmentation and Hypopigmentation:
Benign Pigmented Lesions | 147 |
| Henry H.L. Chan | |

11 Pigmentation and Hypopigmentation: Vitiligo and Other Disorders	157
Thierry Passeron and Jean-Paul Ortonne	
12 Precancerous Conditions and Malignant Tumors	165
Christian Raulin, Syrus Karsai, and Laurenz Schmitt	
13 Scars, Keloids, and Stretch Marks	177
Hilda Justiniano, Andrea Willey, and Suzanne L. Kilmer	
14 Laser Treatment of Tattoos and Other Dyschromia	189
Syrus Karsai and Christian Raulin	
15 Varicose Veins: Endovenous Laser Treatment	211
Serge R. Mordon and Marc E. Vuylsteke	
16 Common Vascular Lesions	227
Emil A. Tanghetti, Mirko Mirkov, and Rafael A. Sierra	
17 Vascular Lesions: Port Wine Stains	241
Sean Lanigan	
18 Vascular Lesions: Hemangiomas	245
Margitta Poetke, Peter Urban, and Hans-Peter Berlien	
19 Rare Vascular Lesions	281
Sean Lanigan	
20 Viral Infections	285
Daisy Kopera	
21 Wrinkles and Acne Scars: Ablative and Nonablative Facial Resurfacing	289
Melissa A. Bogle, Geeta Yadav, Kenneth A. Arndt, and Jeffrey S. Dover	
22 Wrinkles and Acne Scars: Technology-Based Treatment of Periorbital Wrinkles	299
Laurel Naversen Geraghty and Brian S. Biesman	
23 Wrinkles and Acne Scars: Fractional Ablative Lasers	307
Arielle N.B. Kauvar and Melanie A. Warycha	
24 Wrinkles and Acne Scars: Fractional Nonablative Lasers	319
Uwe Paasch	

Part III Special Aspects

- 25 Complications in Laser Surgery and IPL Treatment** 333
Christian Raulin, Syrus Karsai, and Laurenz Schmitt
- 26 Cooling Techniques** 345
Stefan Hammes
- 27 Ethical Considerations in Aesthetic Medicine** 351
Giovanni Maio
- 28 Photodynamic Therapy** 357
Philipp Babilas and Rolf-Markus Szeimies
- 29 Quality Standards in Aesthetic Medicine** 377
Hans-Robert Metelmann, Peter D. Waite, and Stefan Hammes
- 30 Safety/Eye Protection** 383
Wolfgang Bäumlner

Part IV Afterword

- 31 The Business of Laser Surgery** 397
Christopher B. Zachary
- 32 The Hall of Shame** 407
Christopher B. Zachary
- Index** 411

Part
Basics



Core Messages

- › Following the history of lasers and, at the same time, their medical applications demonstrates the continuous improvement of insight into laser reactions and the development of devices.
- › Understanding the characteristics of photons and light is the basis for all applications in medical diagnosis and therapy.
- › Knowledge about the physical principle of lasers will remove any mystery from laser technology.
- › Lasers can be designed in different ways and thus be optimised to the intended use.
- › Laser radiation, depending on the wavelength and the mode of operation, is a powerful tool to treat patients, but it also can be dangerous if safety instructions are ignored.
- › An overview about the different types of medical lasers on the market facilitates the right choice of a laser system for the specific application.

ideas about stimulated emission of radiation [5] was necessary. Albert Einstein developed the theoretical concept of light travelling in waves of particles (photons) and of “stimulated emission.” Although Einstein did not invent the laser his work laid the foundation for it. He pointed out, considering photon statistics, that stimulated emission of radiation could occur (Fig. 1.1).

The precursor to the laser was the MASER (microwave amplification by stimulated emission of radiation). The impetus for the development of the maser was increasing interest in microwave radiation following the utility of it in radar technology. The first maser [22] was created by Townes (published in 1954) who, along with James Gordon and Herbert Zeiger, succeeded in producing an inverted population by isolating excited ammonia molecules. But the first maser, a system with two energy levels, was incapable of continuous output. To achieve continuous output, new systems with more than two energy levels had to be designed. These systems could release stimulated emission of excited atoms without falling to the ground state, thus maintaining a population inversion. Nikolai Basov and Alexander Prokhorov in Moscow first developed this idea. Basov, Prokhorov, and Townes shared the 1964 Nobel Prize in physics for developing the maser concept (Fig. 1.2).

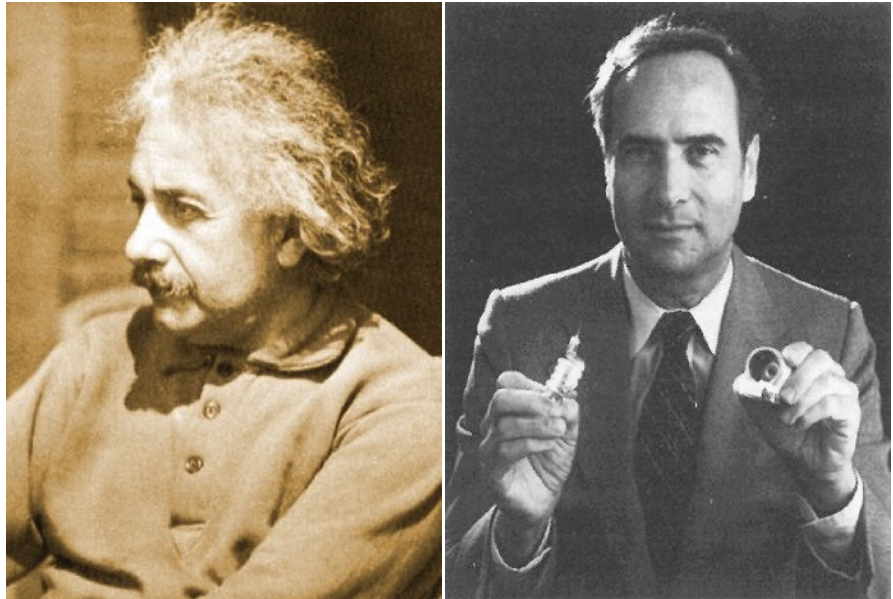
After masers became a reality, scientists looked at the possibility of stimulated emission in other regions of the electromagnetic spectrum. Arthur Schawlow, together with Townes, at Bell Telephone Laboratories in Murray Hill, New Jersey, began investigating the possibility of optical and infrared (IR) masers. They published in 1958 the first detailed proposal for building an optical maser (later to be renamed a laser) in *Physical Review* [10]. The challenges of creating a working laser were tremendous. The much smaller

1.1 History

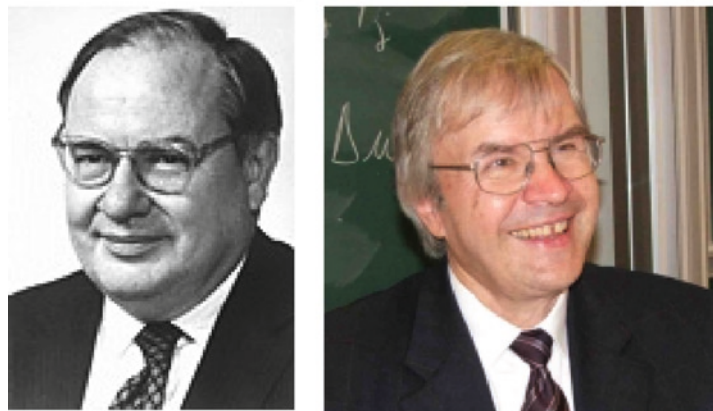
To invent the LASER (acronym for *Light Amplification by Stimulated Emission of Radiation*, coined by Gordon Gould) some understanding of Einstein’s

R. Steiner
Institut für Lasertechnologien in der Medizin und
Meßtechnik an der Universität Ulm, Helmholtzstraße 12,
89081 Ulm, Germany
e-mail: rudolf.steiner@ilm.uni-ulm.de

Fig. 1.1 Albert Einstein (*left*) and T.H. Maiman (*right*)



Alexander M. Prokhorov, Charles Hard Townes, Nicolay G. Basov (1964)



Arthur L. Schawlow (1981) and Theodor W. Hänsch (2005)

Fig. 1.2 Nobel laureates connected with lasers [Alexander M. Prokhorov, Charles Hard Townes, Nicolay G. Basov (1964), Arthur L. Schawlow (1981), and Theodor W. Hänsch (2005)]

wavelengths of visible light and the difficulty of finding an appropriate laser medium meant that many more experiments had to be performed and that it was much more difficult to adjust an apparatus to function as a laser. It was not until 1960 that Maiman [14, 24] created the first working laser. Maiman's laser was a ruby rod with silver ends that had been placed inside a spring-shaped flashlamp. Maiman's laser, however, was only capable of pulsed operation due to its three energy level transitions. Soon afterwards, in 1960, Peter Sorokin and Mirek Stevenson at IBM Laboratories developed the first four-level laser, which was capable, in theory, of continuous output; however, in solid state a continuous output could not be achieved. Further laser developments followed in a short time: the Nd:YAG laser, CO₂ laser, Argon-ion laser, Excimer laser, and diode laser. A list of milestones in the development of lasers is given in Table 1.1.

1.2 Characteristics of Light

Light is electromagnetic radiation in the visible wavelength region from 400 to 700 nm or extended from 380 to 750 nm. Laser radiation, however, is between 100 nm and 1 mm. The speed of light in a vacuum is c (ms⁻¹), where

$$c = 299,792,485 \text{ ms}^{-1} \text{ (or 186,282 miles per second).}$$

Speed of light, the frequency ν of the electromagnetic wave, and the wavelength λ in a vacuum obey the relation

$$c = \lambda \cdot \nu$$

and in matter they obey the relation

$$c(\lambda) = c_0 / n(\lambda)$$

(n = the wavelength-dependent refractive index).

Table 1.1 Milestones in the history of lasers

1917	Einstein publishes his paper about stimulated emission
1951	Development of the maser by C.H. Townes
1958	C.H. Townes and A.L. Schawlow propose that the maser concept could be extended to optical frequencies
1960	T.H. Maiman at Hughes Labs and his assistant Charles Asawa report on May 16 the first functioning laser: a pulsed ruby laser
1961	First medical laser applications in ophthalmology by Charles J. Campbell
1961	The first continuous wave laser is reported by A. Javan: the helium neon laser
1962	First diode laser is reported by M.I. Nathan et al.
1963	First medical laser applications in dermatology by L. Goldman
1964	Nicolay Basov, Charles Townes, and A.M. Prokhorov get the Nobel prize for their fundamental work in the field of quantum electronics, which has led to the construction of oscillators and amplifiers based on the maser and laser principles
1964	The Argon Laser is developed at Hughes Labs. The continuous wave 488/514 nm argon ion laser is well suited to retinal surgery Kumar Patel invents the CO ₂ (carbon dioxide) 10,064-nm (far-infrared) gas ion laser at Bell Labs The Nd:YAG (neodymium doped, yttrium aluminium garnett) 1,064-nm laser also is developed at Bell Labs
1969	The dye laser is introduced at IBM Labs by P. Sorokin and J. Lankard. The pulsed dye laser is the first laser to produce selective light-induced injury
1970	The first excimer laser [based on Xenon (Xe) only] is invented by N. Basov's group at Lebedev Labs, Moscow
1977	J. Madey's group at Stanford University develops the first free electron laser
1980	L. Goldman establishes <i>The American Society for Laser Medicine and Surgery, Inc.</i> , the world's largest professional organization dedicated to promoting excellence in patient care by advancing laser applications and related technologies
1981	A. Schawlow and N. Bloembergen receive the Nobel prize for "their contribution to the development of laser spectroscopy and nonlinear optics"
1984	D. Matthew's group at Lawrence Livermore Labs demonstrates a "laboratory" x-ray laser
2005	J. Hall and T. Hänsch receive the Nobel prize for contributing to the development of laser-based precision spectroscopy, including the optical frequency comb technique

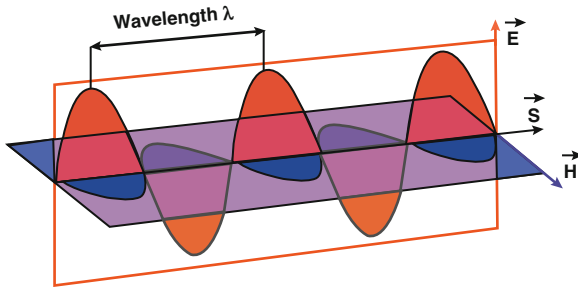


Fig. 1.3 Schematic presentation of an electromagnetic wave with electric, E , and magnetic, H , field vectors and the Poynting vector, S . The planes of the linearly polarised field vectors are perpendicular to each other

The electromagnetic radiation is characterised by Maxwell's equations of an alternating electric field, with field strength E (V/cm) and magnetic field H (Fig. 1.3). The transported power is described by the Poynting vector S (W/m²) representing the energy flux density

$$S = E \times H.$$

According to Bohr's atomic model, electrons occupy certain fixed orbitals (principal quantum number). Electrons can only jump from orbit to orbit and therefore they can emit energy (emission of radiation) or absorb energy (absorption of radiation). The quantisation of energy is described by ΔE (eV). (Fig. 1.4).

$$\Delta E = h \cdot \nu \text{ where } h \text{ is}$$

(h : Planck's constant;

$$h = 6.26617 \times 10^{-34} \text{ Js; } \nu = \text{frequency of light.}$$

With this expression, light can be described either as a wave or as a particle (photon) moving at the speed of light, having no mass but carrying energy and momentum. This property is referred to as wave-particle duality [3, 20]

$$\text{Energy : } E_{\text{photon}} = h \cdot \nu,$$

$$\text{Momentum : } p = E_{\text{photon}} / c = h \cdot \nu / c,$$

$$\text{Power : } P = N_{\text{photon}} \cdot h\nu / t \text{ (} N : \text{number of photons).}$$

1.2.1 Stimulated Emission of Radiation

Photons can be absorbed by atoms when the energy corresponds to an electron transition to a higher energy

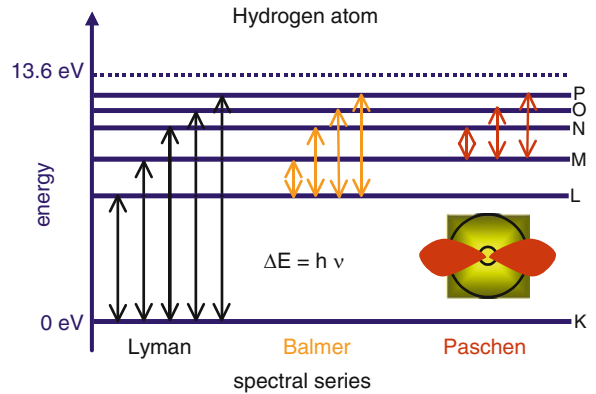


Fig. 1.4 Schematic presentation of the origin of spectral lines of a hydrogen atom

level (orbit). The atom is then in an excited state with energy E_2 . It may spontaneously decay to the ground state, with energy E_1 , emitting a photon with the difference in energy between the two states, $\Delta E = E_2 - E_1 = h\nu$, where h is again Planck's constant. The phase of the spontaneously emitted photon and also the direction of travel are random. This is different for stimulated emission (Figs. 1.5 and 1.6).

The interaction of a photon with an atom will affect the atom's state. The atom, acting as a small electric dipole, will oscillate with the external field. Thus, an electron, due to the presence of another photon, is influenced to decay to the lower energy level, releasing a second photon that is in phase with the first photon. The second photon also travels in the same direction and has the same energy and polarisation. This is called *stimulated emission*. As a result, the two photons are totally coherent. This is also the basis for optical amplification to take place.

If the number of atoms in the excited state is given by N_2 , the rate at which stimulated emission occurs is given by:

$$dN_2 / dt = -B_{21}\rho(\nu)N_2,$$

where B_{21} is a proportionality constant for this particular transition and is also called the Einstein B_{21} coefficient. $\rho(\nu)$ is the radiation density of photons of the frequency ν . The emission rate of photons is therefore proportional to the number of excited atoms, N_2 , and the density of the perturbing photons. For spontaneous emission we have $dN_2/dt = -A_{21}N_2$ and for induced absorption we have $dN_1/dt = -B_{12}\rho(\nu)N_1$.

Fig. 1.5 Absorption and spontaneous emission. A photon is absorbed by an atom, lifting an electron into a higher orbit. This excited state lasts only for about 10^{-7} s, then the electron drops into a lower orbit with emission of a photon of energy $\Delta E = E_2 - E_1$

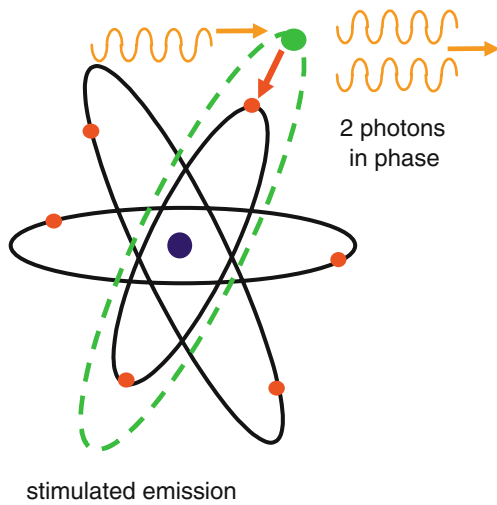
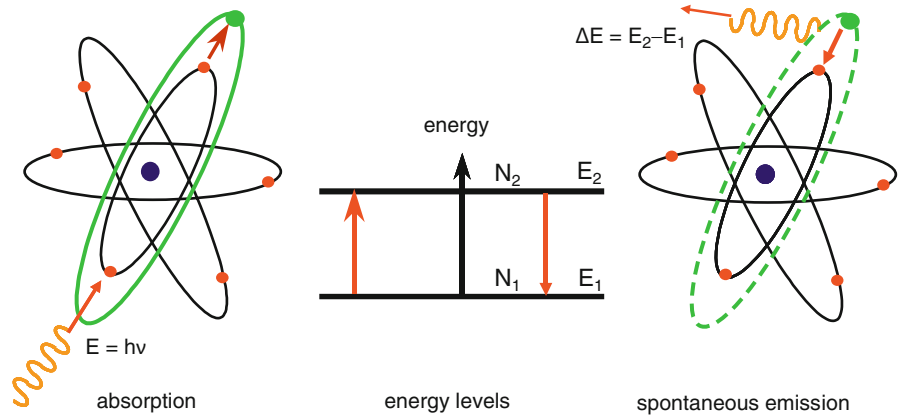


Fig. 1.6 Stimulated emission. A photon induces the decay of an excited energy state. Simultaneously, a second photon is emitted that has the same phase and wavelength

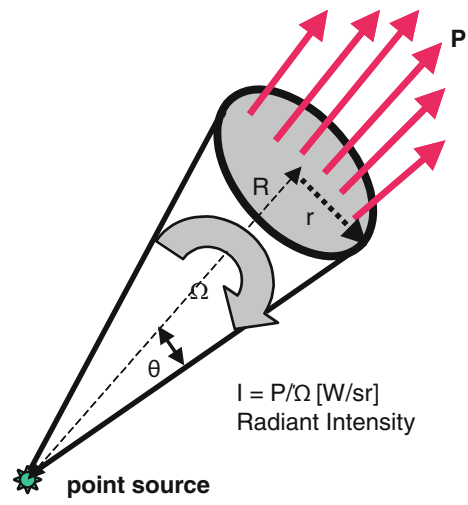


Fig. 1.7 Schematic representation of radiant intensity from a point source

1.2.2 Definitions of Radiation

1.2.2.1 Radiant Power

The power output of a source is described by its *radiant power*, P (W). It is measured with a power or energy metre by photodiode or thermal sensors.

1.2.2.2 Radiant Energy

This is energy emitted, transferred, or received as radiation. A source with a power output P (W), which is turned on for a time duration t (s), will yield a *radiant energy*, Q (J).

$$Q = P \cdot t \text{ (J;Ws).}$$

1.2.2.3 Radiant Intensity

The power P (W) from a point source that is directed into a particular direction at a solid angle, Ω (steradians or sr), is called the *radiant intensity*, I (W/sr).

For an isotropic source, the whole sphere has 4π (sr) of solid angle. In limit of small angle θ , the solid angle of a cone Ω is (Fig. 1.7):

$$\Omega = 4\pi \cdot \pi r^2 / 4\pi R^2 \text{ (sr)} = \pi r^2 / R^2 \text{ (sr)} = \pi \theta^2 \text{ (sr).}$$

1.2.2.4 Irradiance

The power P (W) of a continuously emitting source that irradiates a surface area, A (cm²), is called the *irradiance*, E , where

$$E = P / A \text{ (W/cm}^2\text{).}$$

1.2.2.5 Radiant Exposure

The energy Q (J) of a pulsed light source that reaches a surface A (cm²) due to an irradiance E , and is maintained for a time interval t (s) is called *radiant exposure*, H , where

$$H = Q / A = Pt / A = Et \text{ (J/cm}^2\text{)}.$$

1.2.2.6 Fluence Rate

Imagine an isotropic sphere located in biological tissue collecting photons impinging from all angles onto a small region of its surface. Then it measures the *fluence rate*, F (W/cm²). The fluence rate is the total absorbed power by the small sphere divided by its cross-sectional area, A ($A = \pi r^2$). The fluence rate irradiating the target sphere is:

$$F = P_{\text{absorbed}} / A \text{ (W/cm}^2\text{)}.$$

In some literature the fluence rate is expressed with the greek symbol Φ .

1.3 Principle of Lasers

A laser is actually an *oscillator* rather than a simple amplifier. The difference is that an oscillator has positive feedback in addition to the amplifier. “Light” is understood in a general sense of electromagnetic radiation with wavelengths from 100 nm to 1 mm. Thus one can have ultraviolet, visible, or IR lasers. In medical applications nearly all types of lasers are used for specific medical treatments or diagnostic applications.

The amplifier of a laser is the laser material that can be a solid, a gas, or a liquid. The feedback mechanism is produced by the resonator, where the light is reflected

by two mirrors so that the photons pass several times through the laser material. The number of photons within the resonator increases exponentially due to the stimulated emission (Fig. 1.8).

However, a laser can only work when the stimulated emission of excited atoms of a laser material is larger than the spontaneous emission and the losses within the resonator. In thermal equilibrium, according to the Boltzmann statistics, the number of excited atoms, N_2 , with higher energy, E_2 , is always smaller than the number, N_1 , of atoms in the lower energy level, E_1 . Therefore, a two-level laser system cannot exist because there must be the possibility of an *inversion*. This is possible with a three- or four-level laser design.

The rate balance of a two-level system at thermal equilibrium using the Einstein’s coefficients is

$$\begin{aligned} & \text{(Induced absorption)} B_{12}\rho(\nu)N_1 = B_{21}\rho(\nu)N_2 \\ & \text{(stimulated emission)} + A_{21}N_2 \text{ (spontaneous emission)}. \end{aligned}$$

With the relation of the Einstein coefficients $A_{21}/B_{21} = 8\pi h\nu^3/c^3$, we receive also Planck’s law of black body radiation:

$$\rho(\nu) = 8\pi h\nu^3 / c^3 \times 1 / (e^{h\nu/kT} - 1).$$

The premise for a laser activity is the population inversion between the levels where the laser transition should take place. The higher this inversion, the more effective is the laser. To get a high inversion, the Einstein coefficient A_{21} of the upper laser level should be small so that the losses due to spontaneous emission are small as well. This means that the lifetime of the upper laser level τ_2 should be long. The lower laser level should be less populated (Fig. 1.9) and should have a short lifetime.

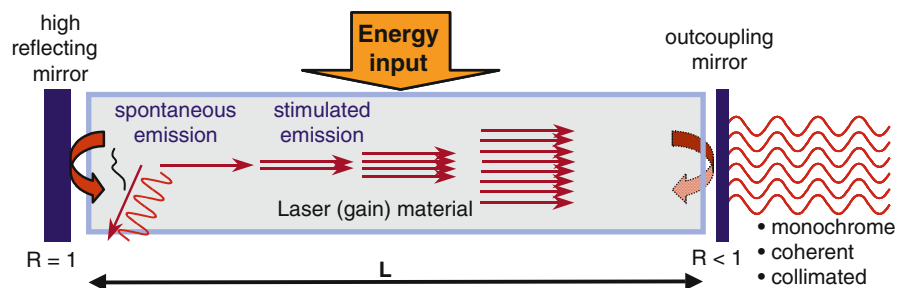


Fig. 1.8 Principle of a laser

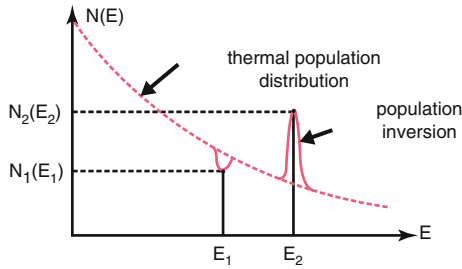


Fig. 1.9 In thermal equilibrium (Boltzmann statistics) the population distribution follows an exponential curve, meaning that the number of excited atoms with higher energy is always less than at lower energy levels ($N_2 < N_1$). Population inversion is the opposite ($N_2 > N_1$)

1.3.1 Laser Design

To produce a population inversion in the laser material of a solid-state laser, one needs a pumping source, which can be a flashlamp or another pumping laser (diode laser). The absorption of the ground state must be sufficiently high. A large Einstein coefficient B is favourable. These conditions are well fulfilled in three-level and four-level systems (see Fig. 1.10).

The first laser, which was demonstrated and produced by Maiman, was a *three-level* ruby laser. Ruby is an Al_2O_3 crystal in which about 0.05% of the Al ions are replaced by Cr^{3+} ions. The problem of a three-level laser is that the lower laser level is the ground state, as shown in Fig. 1.10. It is much more difficult to obtain population inversion in three-level lasers because the lower laser level initially has a very large population, N_0 . By turning on the flashlamp

pump, dN atoms are excited and lifted to level 1, which then decay quickly to level 2. Thus, the population of level 2 will be dN , and the population of the ground state will be $(N_0 - dN)$. Hence, for population inversion we require $dN > (N_0 - dN)$, that is, $dN > N_0/2$. Therefore, to obtain population inversion we have to pump more than half the atoms out of the ground state into the upper laser level. This obviously requires a very large amount of energy, which normally only can be delivered by intensive flashlamps. Therefore, three-level lasers are pulsed lasers. One exception of a three-level continuous wave (cw) laser is the argon ion laser. Here, electrical energy is used to ionise the atoms to become the lower laser level.

Much less energy is required to reach the laser threshold in four-level lasers, in which the lower laser level is empty before the pumping process starts. Although the threshold for population inversion is very high in a three-level system, they can be quite efficient once this threshold is overcome. Ruby lasers pumped by bright flashlamps actually give very high output pulse energies of 20 J easily, and are used in dermatologic applications.

Continuous lasers, like the Nd:YAG laser, normally use four-level systems. Atoms are pumped from the ground state to level 3, which can be composed of different excited states. From there, the upper laser level 2 is populated by fast transition, τ_{32} . This level is long-lived. It is a metastable system because the transition directly to the ground state, τ_{20} , is forbidden. The laser transition occurs to the lower laser level 1 which is short-lived, with fast transition to the ground state. This allows for very efficient pumping.

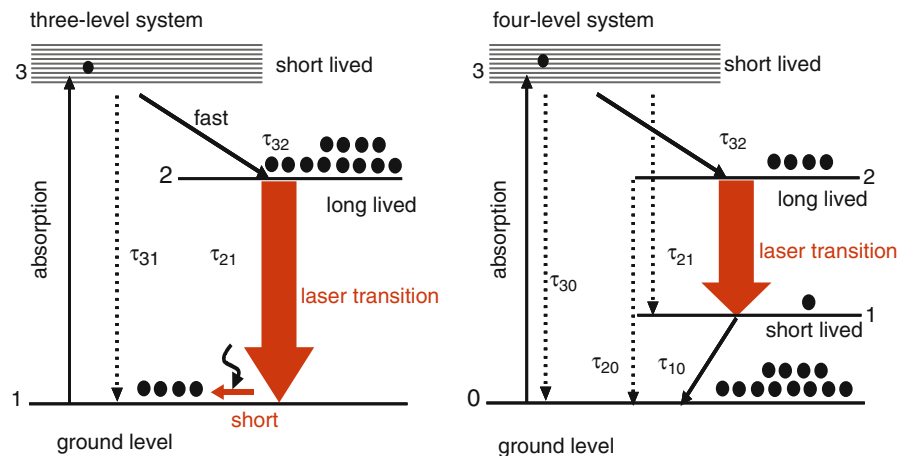


Fig. 1.10 Three- and four-level laser systems

1.4 Optical Resonators

The optical resonator is composed of two mirrors with the laser active medium located between them. The mirrors might either be flat (Fabry-Perot-Resonator) or curved. In case of plane-parallel mirrors, the reflected beam in the resonator is a plane wave. Because mirrors are never ideal plane, this resonator has losses and is slightly unstable. Stable resonator configurations use concave mirrors and are easier to adjust. Oft-used resonator configurations are the symmetric confocal resonator ($R_1 = R_2 = L$), which has the most stable design and least diffraction losses, as well as the spherical type ($R_1 = R_2 = L/2$).

The relation that describes the stability of an optical resonator is determined by the resonator length, L , and the curvatures of the mirrors, R_1 and R_2 . With the mirror parameters

$$g_1 = 1 - L / R_1 \text{ and } g_2 = 1 - L / R_2$$

the stability condition is (Fig. 1.11):

$$0 \leq g_1 g_2 \leq 1.$$

The resonator geometry determines the form of the output beam with regard to diameter, divergence, and

composition of modes. When we consider a stable Gaussian resonator, the multiple reflected beam is always running back in to itself and the phase of the wave front must match the curvature of the mirrors. Because of the marginal condition of the electromagnetic field on the mirrors, a standing wave results along the axis. Therefore, the standing wave spectrum must fulfil the condition:

$$n \cdot \lambda / 2 = L,$$

with integer $n = 1, 2, 3, 4, \dots$;
wavelength λ ; and resonator length L .

This results in an axial spectrum of longitudinal modes with frequency spacing:

$$\Delta\nu = c / 2L.$$

As an example, for a resonator length of 0.5 m, neighboring longitudinal modes are separated by $\Delta\nu = 300$ MHz. A laser emits a characteristic mean wavelength according to the atomic resonance frequency, which is broadened due to the Doppler effect. If pumping of the laser exceeds the threshold because of losses in the resonator, then laser radiation is emitted and the number of longitudinal modes (axial eigenfrequencies) is determined by the ratio of the Doppler width, $\Delta\nu_D$, to the separation of the modes, $c/2L$, as demonstrated in Fig. 1.12.

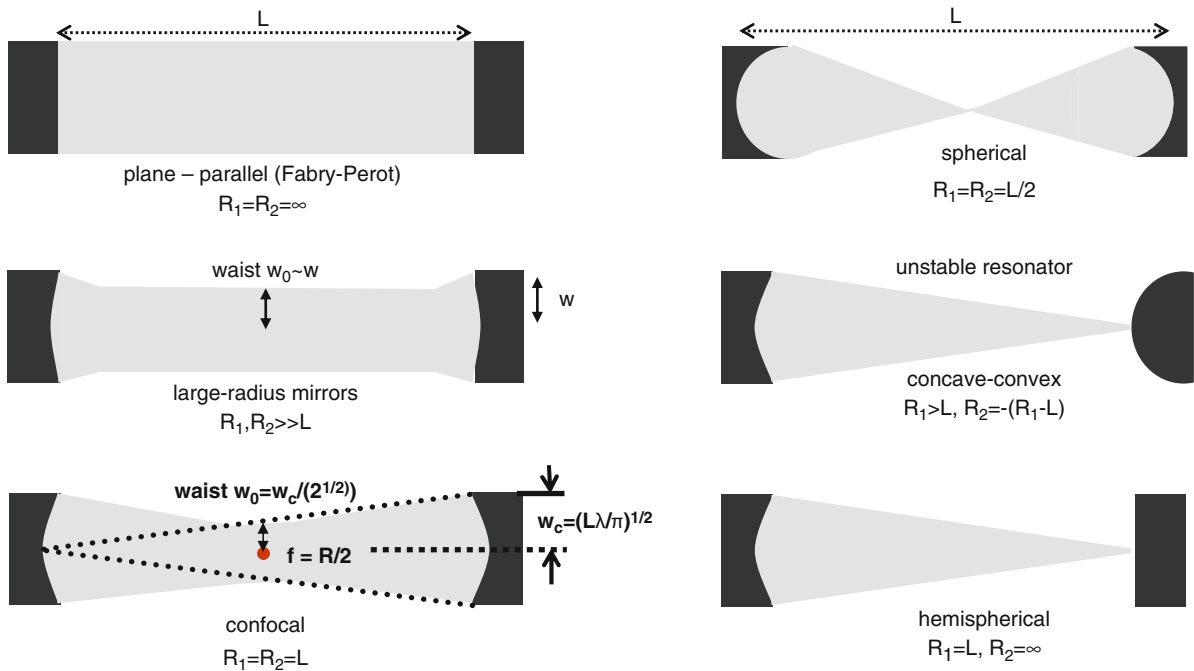


Fig. 1.11 Different stable and unstable resonator configurations

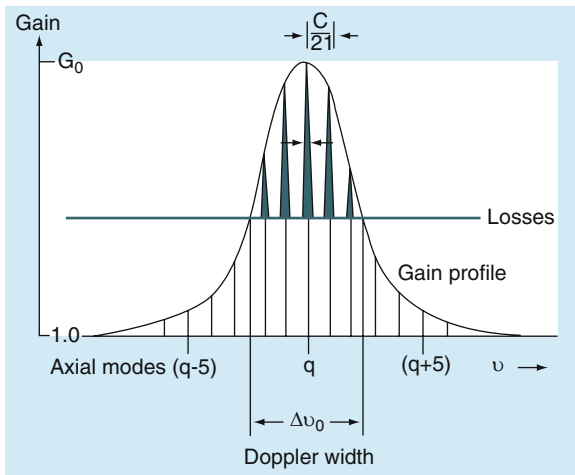


Fig. 1.12 Origin of the longitudinal (axial) modal spectrum. Laser activity is only observed when the gain within the Doppler width exceeds the losses

Practically, only few resonators are working in the stable Gaussian basic mode. Like all systems characterised by marginal conditions, resonators have an entire spectrum of inherent modes. The Gaussian basic mode (Fig. 1.13) represents the oscillation state with the lowest inherent value. Higher modes have a more complex intensity distribution and the transversal expansion of the beam is larger. To increase the output power of a

laser, a large amplification volume has to be generated with the assistance of higher transversal modes.

Resonators using spherical mirrors have an output beam with allowed transversal intensity distributions mathematically described by the Hermite-Gaussian modes, the so-called TEM_{nm} modes (transversal electromagnetic modes). Lasers are often designed for the operation in a single transversal mode, the basic Gaussian mode TEM_{00} , which has the smallest beam diameter and the smallest spot size in the focus. Normally they have cylindrical symmetry. In this case the transverse mode patterns are described by a combination of a Gaussian beam profile with a Laguerre polynomial. The modes are denoted TEM_{pl} , where p and l are integers representing the radial and angular mode orders, respectively.

With $p = l = 0$, the TEM_{00} mode is the lowest order, or the fundamental transverse mode of the laser resonator, and has the form of a Gaussian beam (Fig. 1.14). The pattern is a round spot with a constant phase. Modes with increasing p show concentric rings of intensity, and modes with increasing l show angularly distributed lobes. In general there are $2l(p+1)$ spots in the mode pattern. The overall size of the mode is determined by the Gaussian beam radius w , and this may increase or decrease with the propagation of the beam. During propagation the modes preserve their general

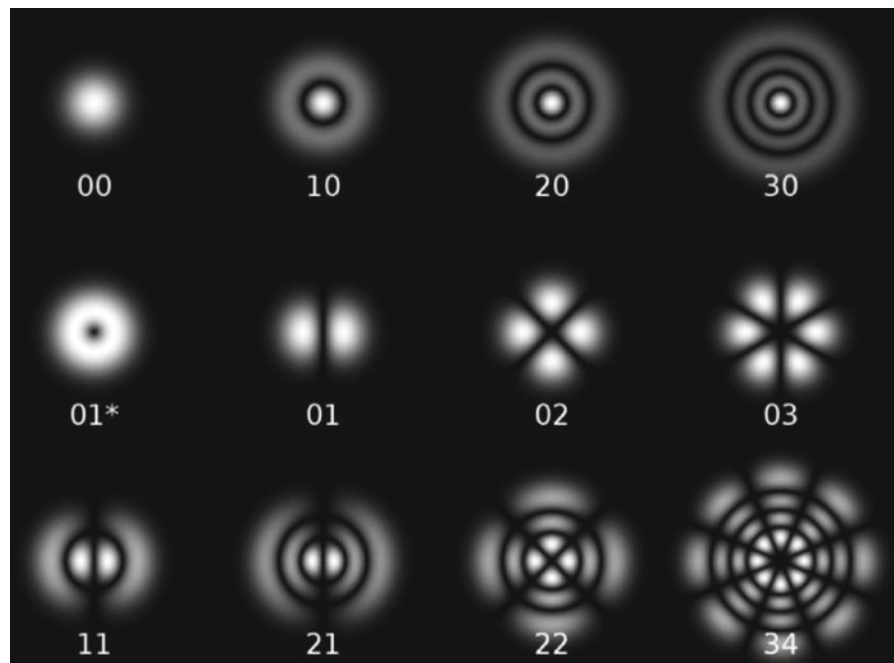
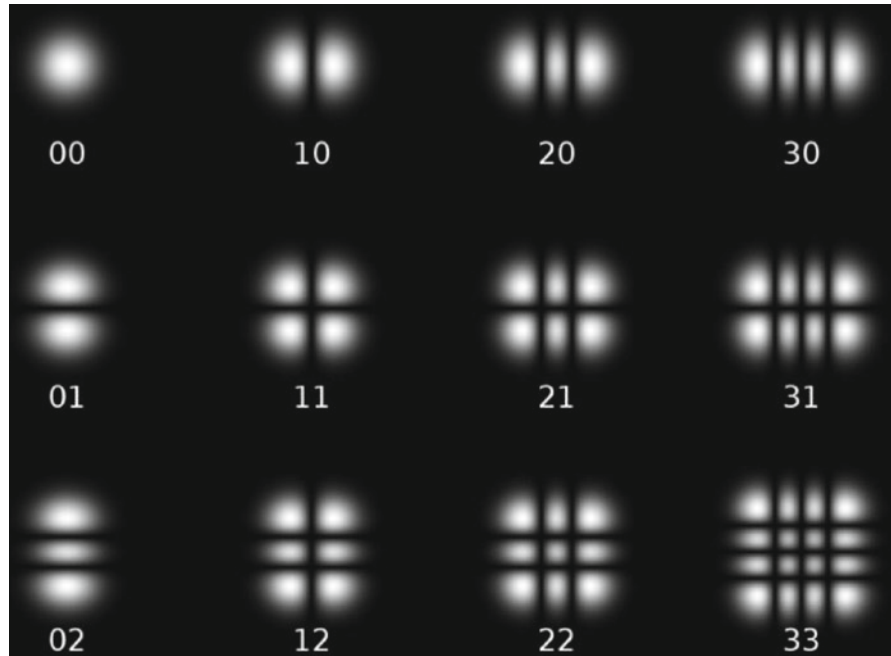


Fig. 1.13 Cylindrical transverse mode patterns TEM_{pl} . TEM_{01} represents a special case, the so-called *doughnut mode*, an overlay of the patterns with $l = 1, 2, 3$

Fig. 1.14 Rectangular transverse mode pattern TEM_{mn} of lasers with Brewster's angle elements



shape. Because higher-order modes are larger compared to the TEM_{00} mode, the fundamental Gaussian mode of a laser may be selected by placing an appropriately sized aperture in the laser cavity that only the fundamental mode can pass through.

The symmetry of optical resonator often is restricted in lasers by polarising elements like Brewster's angle windows, leading to transverse modes with rectangular symmetry. These modes are named TEM_{mn} , with m and n being the horizontal and vertical orders of the pattern. The intensities of the patterns are determined by the order of the Hermite polynomials and demonstrated in Fig. 1.14. The TEM_{00} mode corresponds to the same fundamental mode as in the cylindrical geometry. The number of spots in the intensity patterns is described by the expression $(m+1)(n+1)$. The polarisation of the phase in each spot is offset by π radians with respect to the horizontal or vertical neighbours.

1.5 Laser Radiation

Laser radiation is characterised by its parallelism, the spatial and temporal coherence; its monochromatism, the spatial distribution and divergence (beam quality); and the polarisation, power, and operating mode (pulsed or cw).

The intensity distribution across a Gaussian beam is a bell-shaped Gaussian function. It is a beam of best

quality that can be focused to the smallest spot. Lasers emitting in TEM_{00} mode have such a quality. The Gaussian function of the intensity $I(r,z)$ depends on the distance, z , from the beam waist and the radius, w , according to the formula:

$$I(r,z) = I_0 (W_0 / W(z))^2 \exp^{-2r^2/W^2(z)}.$$

The intensity at the beam waist, I_0 , can be described in relation to the laser power, P , by the expression:

$$I_0 = 2P / \pi w_0^2 \text{ (W/cm}^2\text{)}.$$

With distance, z , from the beam waist at z_0 , the cross-section and the radius, w , of the beam increases and can be expressed as

$$w(z) = w_0 (1 + (z/z_0)^2)^{1/2}.$$

The distance, z , where the cross-section of the beam is twice the area of the focal spot is called the *Rayleigh length* (see Fig. 1.15).

$$\text{Rayleigh length : } z_0 = \pi w_0^2 / \lambda$$

where the beam has widened to:

$$w(\pm z_0) = w_0 \sqrt{2}.$$

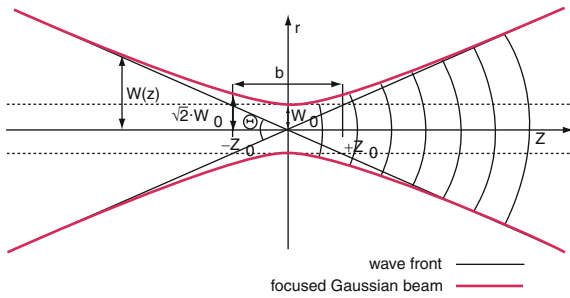


Fig. 1.15 Focused Gaussian beam with spherical wave fronts and the angle of divergence Θ . The radius of the beam waist is w_0 and at a certain distance from the beam waist, $w(z)$. The distance until $\pm z_0$ is twice the Rayleigh length, b

The length between the spots $\pm z_0$, denominated as b , is twice the Rayleigh length and is called the *confocal parameter*. The intensity there is half the intensity at the focal spot.

The quality of multimode laser beams, which have no Gaussian profile, is expressed as M^2 , which is independent of λ . It is the relation of the beam parameter product (BPP), which is the product of a laser beam's divergence angle (half-angle) and the radius of the beam at its narrowest point (the beam waist), to that of a Gaussian beam. The BPP quantifies the quality of a laser beam and how well it can be focused to a small spot. M^2 of a Gaussian beam is exactly one. The smaller M^2 of a laser beam is, the smaller is its focal spot.

$$M^2 = w\Theta / (\lambda / \pi)$$

with the divergence of a Gaussian beam,

$$\Theta_0 = \lambda / \pi w_0.$$

If the waist of a laser beam is equal to that of a Gaussian beam, then

$$M^2 = \Theta / \Theta_0.$$

Important laser parameters are summarised in Table 1.2.

Polarisation of the laser beam can be achieved by introducing polarising optical components into the resonator, such as deflecting mirrors in folded resonators or by active laser crystals where the faces have Brewster angles (Fig. 1.16). Such a Brewster resonator produces linear polarised light. The disadvantage may be that the losses of the resonator increase and the output power is reduced.

Table 1.2 Important laser parameters

Wavelength λ (nm or μm)	Photon energy
Power P (W)	For cw lasers
Energy $E = Pt$ (J)	For cw lasers
Peak power P_{max} (W)	For pulsed lasers
Energy E per pulse (J)	For pulsed lasers
Pulse duration t [fs (10^{-15}) to ms (10^{-3})]	For pulsed lasers
<i>Effect on tissue</i>	
Energy density E/A (radiant exposure) (J/cm^2) (A = effective area)	For pulsed lasers
Power density W/A (irradiance) (W/cm^2) (A = effective area)	For cw lasers
Beam quality $L_w = 1/M^2$ (mm mrad^{-1})	General for lasers

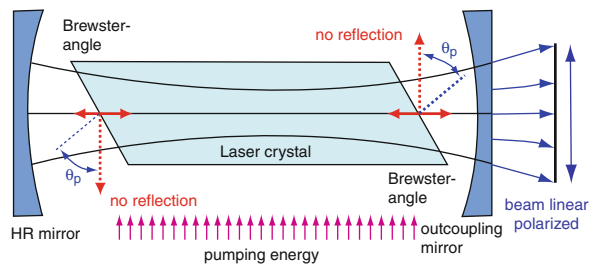


Fig. 1.16 Brewster resonator producing linear polarised laser light [8]

The *operational modes* of lasers are cw, pulsed as interrupted radiation (in ms), pulsed free running (in hundreds of μs), Q-switched (in ns), or mode-locked (in fs).

Interrupted radiation of a cw laser is done by mechanical or electronic switching with modification of the pulse length. The pulse frequency is low to moderate, up to 100 Hz. Flashlamp-pumped solid-state lasers in the free-running mode have pulse lengths of 50 μs up to several hundred microseconds. Pulses of medical dye lasers systems can vary from microseconds to 50 ms.

Shorter pulses with very high intensities in the nanosecond range are produced by Q-switching of the laser. A Q-switch can be introduced into the resonator that reduces the performance factor of the laser resonator. Therefore, the threshold for lasing is very high for a short period of time. During this time, with continuous

pumping, pumping power, P_p , the inversion of the number of excited atoms, can be built up, $\Delta N(t)$ (Fig. 1.17). When the Q-switch opens at $t=0$, the threshold power, $S(t)$, goes down immediately and the amplification is now much higher than the resonator losses. A strong laser pulse is generated with complete depletion of the energy reservoir [21].

The power of the pulse can be estimated according to the expression:

$$P(t) = h\nu T(c/2L)Vn(t) \text{ (W)},$$

where h is Planck's elementary quantum of action (Planck's constant), ν is the frequency of the laser transition, $T = 1 - R$ is the transmission of the output mirror, V is the resonator volume, $n(t)$ is the photon number density, and L is the resonator length.

Some typical representatives of Q-switches are shown in Table 1.3.

Ultrashort laser pulses are generated by mode-coupling due to the coherence properties of the laser. Compared to Q-switching, where the shortest pulse durations are in the range of the resonator period, mode-coupling can generate even shorter laser pulses. Mode-coupling finally is attained by forcing a fixed phase relationship, $\Phi_{q+1} - \Phi_q = \Phi$, between the longitudinal laser modes having the distance $\Delta\nu_{q,q+1} = c/2L$

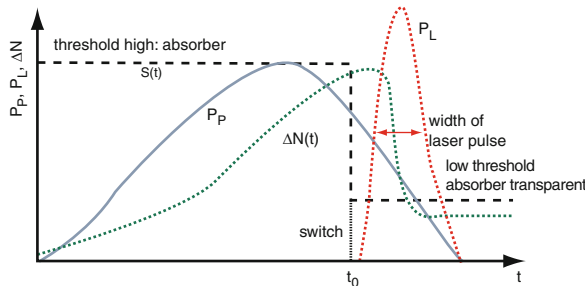


Fig. 1.17 Scheme of a Q-switch: P_p is pumping power, $S(t)$ is threshold power, $\Delta N(t)$ is the inversion, and P_L the laser power

Table 1.3 Typical representatives of Q-switch devices

Type of Q-switch	Switching time
Rotating aperture in resonator	$>10 \mu\text{s}$
Rotating mirror or prism	$<0.1 \mu\text{s}$
FTIR Q-switch	$<50 \text{ ns}$
Electro-optical switch	$<10 \text{ ns}$
Acousto-optical switch	$<50 \text{ ns}$
Saturating absorber	$<0.1 \text{ ns}$

FTIR frustrated total internal reflection

(see Fig. 1.12). This is associated with interference effects with amplitudes that are larger than those of individual modes. For more information see [4].

1.6 Medical Lasers

Since the invention and commercial availability of lasers, such systems have been widely used for medical applications in the treatment of soft and hard biological tissue, from the Ultraviolet (UV) Excimer laser, ArF at 193 nm, in ophthalmology up to the CO_2 laser in the IR-region at 10,640 nm for surgical interventions. The whole spectrum of lasers is shown in Fig. 1.18.

1.6.1 Solid-State Lasers

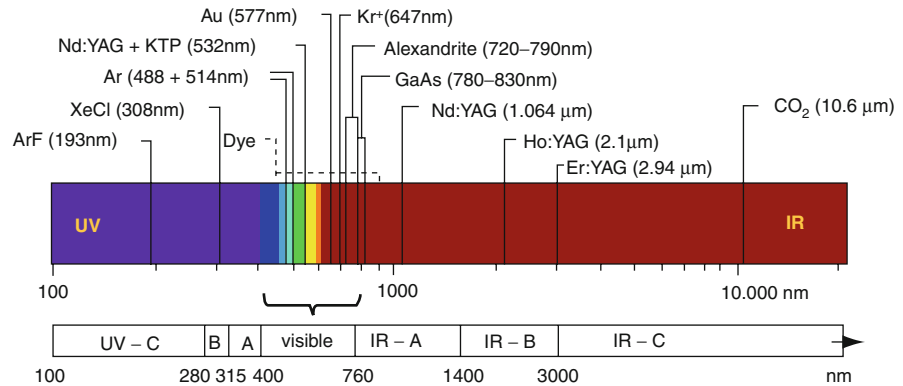
1.6.1.1 Nd:YAG Laser

The most important solid-state laser is the Nd:YAG laser, with neodymium as laser ion (Nd^{3+}) doped with 1–1.5% into an yttrium-aluminium-garnet crystal ($\text{Y}_3\text{Al}_5\text{O}_{12}$). Its fundamental wavelength is 1064.2 nm. Frequency doubling with a KTP crystal (potassium titanium oxide phosphate, KTiOPO_4) leads to 532 nm (green light). The third and fourth harmonics are 355 and 266 nm, respectively. The Nd:YAG laser is a four-level system (Fig. 1.10). Other, weaker emission wavelengths are 1,320 and 1058.2 nm (Nd:CaWO_4). The overall efficiency of a flashlamp-pumped Nd:YAG laser is less than 2%. Therefore, it must be cooled with water. Diode pumped systems (805-nm laser diodes) reach efficiencies of about 15% at output power of about 10–15 W. Nd:YAG lasers are used as cw lasers up to 100 W for surgical applications, e.g., long pulse lasers in dermatology or Q-switch lasers with 20-ns pulse length in urology (lithotripsy) and dermatology (tattoo removal).

1.6.1.2 KTP Laser

KTP lasers are frequency-doubled Nd:YAG lasers using KTP crystals inside the cavity or externally with an emission wavelength of 532 nm in the green part of the visible spectrum.

Fig. 1.18 Medical lasers



1.6.1.3 Er:YAG Laser

The Er:YAG laser with a 2.94- μm wavelength is well suited for ablation of soft and hard biological tissue because the wavelength is highly absorbed in water ($\mu_a = 10^4 \text{cm}^{-1}$). Erbium ions are doped in high concentration (~50%) in YAG or other crystals (Er:YSGG: 2.78 μm ; Cr:Er:YSGG: 2.80 μm ; Cr:Tm:Er:YAG: 2.64 μm). This laser exists only as pulsed laser system because the rather complex energy-level scheme of erbium with important energy-transfer upconversion (ETU; see Fig. 1.19) and cross-relaxation (CR) processes. Laser transition occurs from the energy level $^4I_{11/2}$ to $^4I_{13/2}$. The lower laser level has a longer lifetime of 9 ms compared to the upper laser level. Only by hard pumping and the efficient upconversion processes is lasing possible. The ETU process ($^4I_{13/2}, ^4I_{13/2} \rightarrow ^4I_{15/2}, ^4I_{9/2}$) leads to a fast depletion of the lower laser level. The other advantage of the ETU process is that half of the ions undergoing this process are upconverted to the $^4I_{9/2}$ upper level and, by subsequent multiphonon relaxation, are recycled to the $^4I_{11/2}$ upper laser level, from where they can each emit a second laser photon [18, 19].

Pulsed Er:YAG laser systems (pulse lengths from 100 to 500 μs) have a mean power of up to 30 W and repetition rates of up to 50 Hz, with efficiencies of 1–2%. They are used in dermatological applications for superficial tissue ablation, in dentistry, and in minimal invasive surgery. The laser light is transmitted either by an articulated arm or by fibres. Germanium oxide fibres proved to be stable in clinical routine work.

1.6.1.4 Holmium:YAG Laser

Flashlamp- or diode-pumped Ho:YAG lasers can be operated in the pulsed or the cw mode. In the pulsed

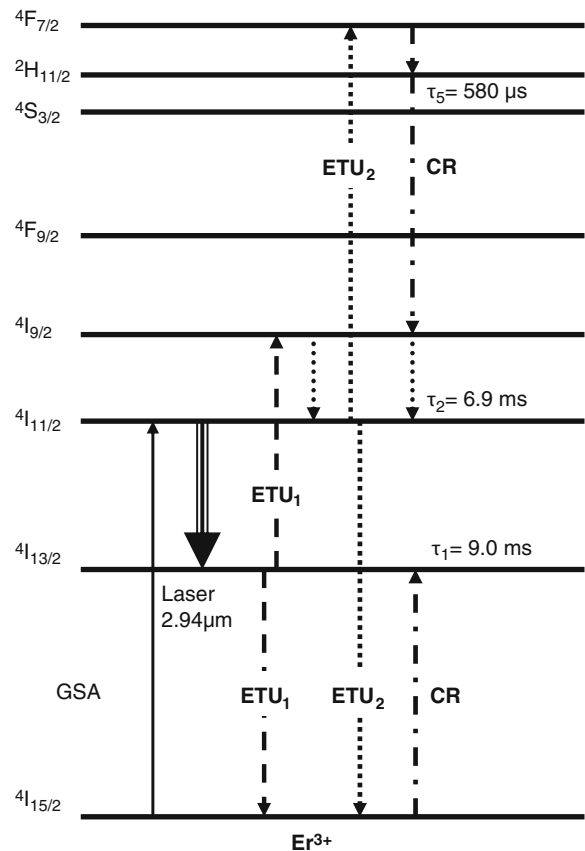


Fig. 1.19 Energy level scheme of the Er:YAG laser. GSA ground state absorption; ETU energy-transfer upconversion between neighboring erbium ions; CR cross-relaxation

mode, with pulse durations 200–600 μs and energies from 0.2 to 3.5 J, repetition rates up to 50 Hz have a mean power of 30–40 W. Combining several laser heads, high-power systems are also available. The wavelength is 2,080 nm.

Applications with low power first appeared in ophthalmology for refractive surgery procedures called

laser thermal keratoplasty to correct mild to moderate cases of hyperopia and astigmatism. In recent years applications in urology and endourology are more important. Besides stone disintegration, treatment of benign prostate hyperplasia (BPH) by enucleation or vaporisation has become a standard surgical intervention [11, 13].

The most efficient laser material for high-power flashlamp-pumped lasers is Cr,Tm,Ho:YAG. The laser's active ion is Ho^{3+} with a concentration of about 0.5% atomic units (AU) in the host material YAG, co-doped with thulium ions (Tm^{3+} , 6% AU) and for lamp pumping with chromium ions (Cr^{3+} , 1% AU). The scheme of the lamp-pumped holmium system is shown in Fig. 1.20.

The pump light in Fig. 1.20 is absorbed by the broad absorption bands $A_2 T_2$ of the chromium ions at wavelengths of 420 and 600 nm or directly by energy levels of the Tm^{3+} ions from 3H_6 3F_4 by diode pumping. From all the excited levels, rapid radiationless energy transfer occurs to the energy level 3F_4 of the holmium ions. The highly excited Tm^{3+} ions are deactivated from the 3F_4 to the 3H_4 level. The energy difference of the levels 3F_4 and 3H_4 fit very well with the energy difference between the low energy level 3H_6 and the 3H_4 level of the Tm^{3+} ion. So the energy of the deactivated Tm^{3+} ion is, with a high probability, resonantly transferred to a neighboring Tm^{3+} ion, which then is excited from the low energy level 3H_6 to the 3H_4 level. This resonant energy transfer is called cross-relaxation with quantum efficiency raised to two. One pump photon can excite two Tm^{3+} ions to the 3H_4 level by this cross-relaxation.

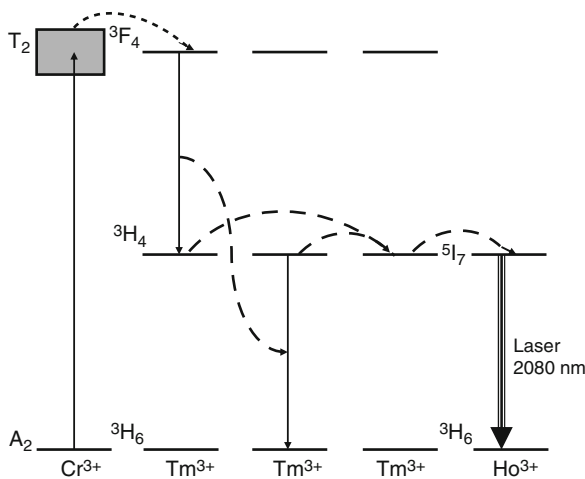


Fig. 1.20 Scheme of the Cr,Tm,Ho:YAG laser system

The 3H_4 excitation energy migrates between neighbouring Tm^{3+} ions via energy resonant processes. If a holmium ion is reached, the energy can be transferred without radiation to the quasi-resonant upper laser level 5I_7 of the Ho^{3+} ion. The laser radiation terminates at the 5I_8 level of the Ho^{3+} ion.

The lower laser level of the Ho^{3+} ion has only a small energy difference to the ground state and is therefore highly populated at ambient temperatures. Holmium laser systems operating at room temperature are quasi-three-level laser systems. Consequently, a very high excitation energy is necessary to reach a population inversion. The resulting thermal load to the laser material in lamp-pumped systems allows laser operation only in the pulsed mode. The laser output is very temperature-dependent. It will be reduced by about 3% per degree of rising temperature.

1.6.1.5 Thulium Laser (Tm:YAG)

Laser therapy of symptomatic BPH is a promising, less invasive alternative to the traditional BPH surgery. Besides the holmium laser, the cw thulium laser at a 2- μm wavelength is used as well [6]. Compared to the KTP laser, the thulium laser is more efficient [25]. The absorption coefficients of the mid-IR lasers are compared in Fig. 1.21. Tm:YAG lasers have a slightly higher absorption in water than the Ho:YAG lasers. Therefore, Tm:YAG lasers are well suited for vaporisation of the prostatic tissue.

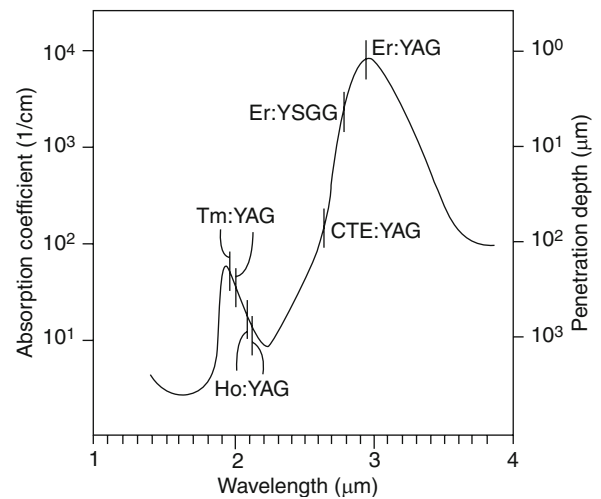


Fig. 1.21 Absorption coefficients and penetration depths in water of mid-infrared laser [7]

1.6.1.6 Alexandrite Laser

This solid-state laser is tunable in the wavelength range 700–830 nm, normally being operated at 750 nm. Alexandrite laser medium is a chromium-doped chrysoberyl ($\text{Cr}:\text{BeAl}_2\text{O}_4$, gemstone alexandrite) and can operate in cw (up to 100 W) or pulsed mode. Because light of this wavelength region is absorbed by melanin and dyes, but not significantly by blood, it can be used for the destruction of melanin-containing structures (hair roots, pigmented lesions). The first applications were reported in the fragmentation of kidney stones [17].

Also not a true four-level laser, the vibronic transition on which this laser usually operates permits operation similar to a four-level laser. The scheme of the energy levels is shown in Fig. 1.22.

The four-level laser depicted in Fig. 1.22 has a ground manifold, a pump manifold, and an upper laser manifold, similar to a three-level laser. But, in contrast to the three-level system, there is a fourth manifold, the lower laser manifold, in which the lower laser level resides, well above the ground manifold. Because the population density of the ground level does not have to be overcome, $\text{Cr}:\text{BeAl}_2\text{O}_4$ operation on a vibronic transition resembles the operation of a four-level laser with a low laser threshold.

1.6.1.7 Ruby Laser ($\text{Cr}^{3+}:\text{Al}_2\text{O}_3$)

Although the ruby laser was the first laser, which was developed by Maiman in 1961, it was for a long time ignored and not used in medical applications. The

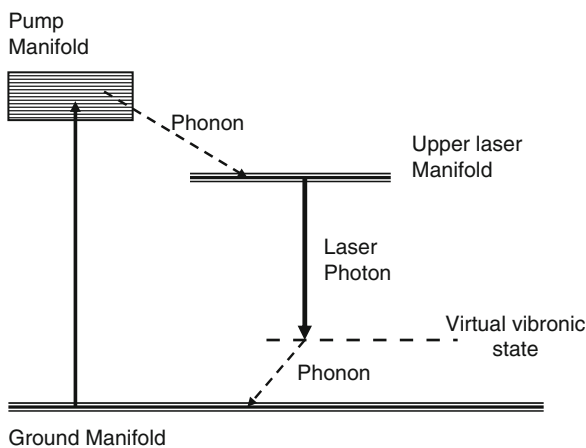


Fig. 1.22 Scheme of the energy levels of the alexandrite laser

emission wavelength is 694 nm. The laser is a three-level laser and therefore more than 50% of the ions in the ground state must be excited to get an inversion. Only strong pumping by powerful flashlamps can produce this inversion. Modern laser systems with advanced technology are able to produce high pulse energies up to 20 J. The laser light is transmitted through fibres or articulated arms. The deep red color of the laser light is absorbed by melanin and dark pigments. Therefore, the medical applications are mostly in dermatology, similar to the alexandrite laser, to remove hairs or tattoos with black or blue color.

The laser active ion is Cr^{3+} replacing Al ions, Al^{3+} , in the host material, sapphire (Al_2O_3), at a doping concentration of 0.05% AU of Cr_2O_3 . The two strong absorption bands in the ruby crystal are around 400 and 550 nm. Optical pumping occurs from the ground state, ${}^4\text{A}_2$, to the two excited states of the chromium ion, ${}^4\text{T}_1$ and ${}^4\text{T}_2$, from where, quickly and without radiation, the energy is transferred to the upper laser level, E . Laser emission of 694 nm occurs from energy level E to the ground state ${}^4\text{A}_2$.

1.6.1.8 Titanium-Sapphire Laser ($\text{Ti}:\text{Al}_2\text{O}_3$)

The Ti:sapphire laser was developed by Moulton and first reported by him in 1986 [15]. This solid-state laser is pumped by a frequency-doubled Nd:YAG laser and can be tuned between 660 and 1,160 nm. With mode-locking the laser emits ultra-short femtosecond pulses (45–180 fs) at high repetition rates (80–100 MHz) or picosecond pulses. Due to the high power of the laser pulses, Ti:sapphire lasers are used as a light source in two-photon microscopy or in ophthalmology for cutting transparent ocular tissue (flap preparation of the cornea for vision corrections).

1.6.2 Gas Lasers

1.6.2.1 Carbon Dioxide Laser

The carbon dioxide (CO_2) laser is still one of the important lasers used for medical surgery and industrial applications. With a power range from mW to tens of kW in the cw mode and an efficiency of up to 30%, laser systems are compact and economic. The sealed laser tube

is filled with a mixture of gases, CO₂ (1–9%), N₂ (13–45%), and helium (60–85%). Excitation occurs by direct current high-voltage gas discharge or through high frequency (RF). It must be mentioned that only with direct current supply units is the superpulse technique possible; it generates pulses <1 ms and with a peak power about ten times higher than the mean power. The gas components have different reaction mechanisms during the laser process.

The structure of the CO₂ molecule is linear, with the carbon atom in the centre. Such molecule configurations can vibrate in symmetric and asymmetric stretch modes as well as in bending modes (Fig. 1.23). The energies associated with molecular vibration are quantised just like electron energies; therefore, only certain vibrational levels are possible. The possible forms of resonant vibration are referred to as the vibrational modes of a molecule.

During gas discharge free electrons collide with N₂ molecules and excite them. The CO₂ is excited through a collision with excited N₂ molecules. This transfer of energy occurs by a resonant effect. Because the vibrational energy levels of N₂ are metastable and have an energy very close to that of the first energy level of the asymmetric stretch mode of CO₂, they have ample time to transfer their energy and excite the CO₂ molecules. The lasing occurs when CO₂ in the excited asymmetric

mode makes the transition to the bending or symmetric stretch modes. The CO₂ then returns to its ground state through another collisional transfer of energy with the helium atoms. With this lasing process the CO₂ laser is a three-level laser with direct pumping into the upper laser level because the lower laser level is depleted very quickly through the presence of helium in high concentration. One receives a bunch of laser lines around the central laser wavelengths at 10.6 and 9.6 μm.

A special variant of the CO₂ laser is the TEA (Transversely Excited Atmospheric Pressure) CO₂ laser. High peak powers can only be achieved by increasing the density of the excited CO₂ molecules. To avoid too high voltage necessary to achieve gas breakdown in longitudinal configuration, Beaulieu invented the TEA-laser in 1970 [2]. Mechanical Q-switching of CO₂ lasers to generate <1 μs pulses at kHz repetition rates can be used to cut bone tissue [12].

Transmission of the CO₂ laser light usually is provided by an articulated arm with mirrors. A new fibre technology invented at Massachusetts Institute of Technology, Cambridge, MA, USA, and developed by OmniGuide Inc., a wavelength-scalable hollow optical fibre from 750 nm to 10.6 μm with large photonic bandgaps [23] opens the possibility of flexible CO₂ laser transmission and endoscopic applications.

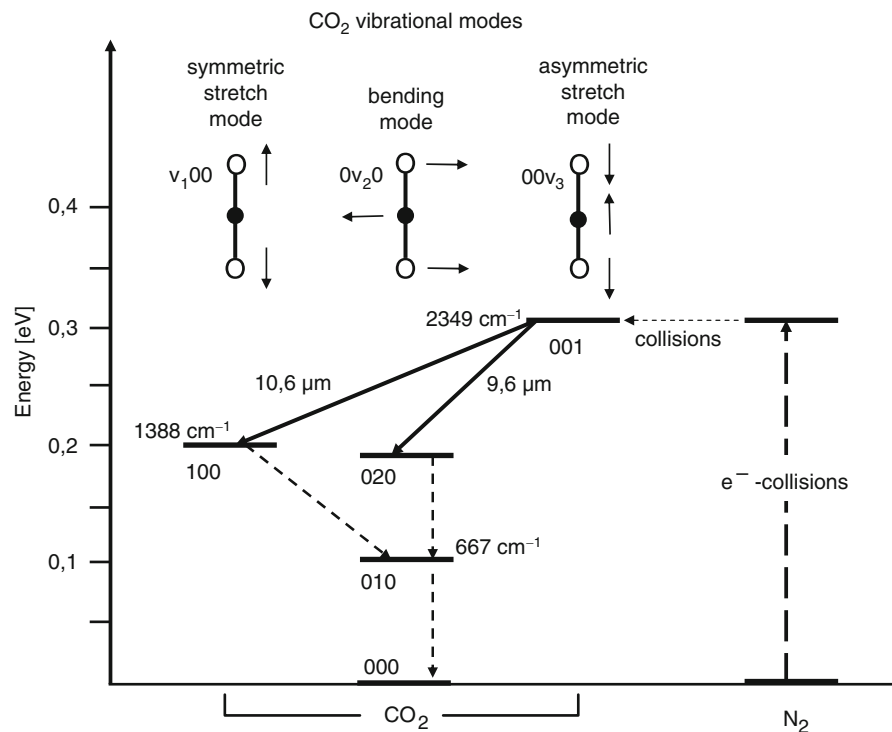


Fig. 1.23 Scheme of the energy levels of a CO₂ laser and the vibration modes of the linear CO₂ molecule

1.6.2.2 Argon Ion Laser

Noble gas ion lasers are cw lasers. Prominent representatives are the Ar^+ laser and Kr^+ laser. The wavelengths of the Argon ion laser are 363, 488 and 514.5 nm in the UV, blue, and green spectral regions. Intense lines of the Krypton ion laser are at 530.9 nm, 568.2 nm, and in the red region are at 647 and 676.4 nm. The output power in multi-line mode of the Ar^+ laser is between 2 and 100 W; the Kr^+ laser has about 20 W. Only in the UV spectrum is the Ar^+ laser still unrivaled.

Ion lasers are very inefficient: about one-tenth of a percent of electrical current is converted to laser light. They need high electrical current supply and water cooling. Nevertheless, the Ar^+ laser has been used to pump Ti-sapphire and dye lasers. It mostly has been replaced by more efficient frequency-doubled Nd:YAG lasers.

The argon laser consists of a plasma tube filled with argon gas at low pressure, 0.01–0.1 mbar. Plasma discharge current up to 60 A ionises the argon from its Ar ground state, $3p^6$, by successive electron collisions to the ionised Ar^+ ground level, $3p^5$. Further electron collisions excite the argon ion to the Ar^+3p^4p (upper laser) levels. Laser transition occurs from these levels to the lower laser levels, Ar^+3p^4s .

1.6.2.3 Helium-Neon (HeNe) Laser

The best known cw gas laser is the HeNe laser. The active medium is a mixture of helium and neon in proportions of 5:1–10:1 at low pressure (1 mbar) in a glass capillary. The actual laser transition occurs in the neon. The gas discharge tube operates at 1.5–2 kV, maintaining a glow discharge or plasma. Electron collisions excite helium atoms from the ground level to the 2^1S_0 and 2^3S_1 state. The energy of the helium atoms is transferred by collision with the neon atom to the neighboring energy levels of the neon, $3s_2$ and $2s$ levels. The $3s_2$ level of neon is an example of a metastable atomic state, meaning that it is only after a relatively long period of time – on atomic time scales – that the $\text{Ne}^*(3s_2)$ atom de-excites to the $2p_4$ level by emitting a photon with a 632.8-nm wavelength. The excited $\text{Ne}^*(2p_4)$ atom rapidly de-excites to its ground state by emitting additional photons or by collisions with the plasma tube walls. Because of the extreme quickness of the de-excitation process, at any time in the HeNe plasma there are more neon atoms in the $3s_2$ state than there are in the $2p_4$ state, and a population inversion is said to be established between these two energy levels.

Further laser lines of the HeNe laser are at 543, 594, 604, and 612 nm in the visible spectrum and at 1,152 and 3,391 nm in the IR spectrum. HeNe lasers are often used as aiming beams, for spectroscopic or diagnostic applications and biostimulation. Maximum output power is 100 mW; small devices have 1–5 mW output power.

1.6.2.4 Excimer Laser

Basov and his colleagues in Moscow first discovered in 1971 the stimulated UV emission of an excited xenon dimer (Xe_2) at 176 nm [1]. Excimer is a short form of the expression “excited dimers.” Molecules, such as noble gas halides (ArF , KrF , XeCl , XeF), are stable only in their excited states and not in their ground states. The laser medium consists of such molecules in a buffer gas like helium or neon at a total pressure of 2–3 bar.

Figure 1.24 shows the potential curves of for a halogen rare gas molecule, (RGH) in its excited state and ground state. The electronically excited RGH (XY^*) forms the upper laser level with a lifetime of several nanoseconds. The laser radiation occurs during transition from this excited state to the non excited state of rare gas and halogenide. The efficiency of excimer lasers is about 2%. They exist only as pulsed lasers, with pulse widths ranging from several ns to 100 ns. Maximum mean power is 200 W. The repetition rate is up to kHz.

The wavelength of an excimer laser depends on the rare gas and the halogenide. The wavelengths mainly used in the UV spectrum are listed in Fig. 1.25.

1.6.3 Dye Lasers

The invention of the dye laser in 1966 by Fritz P. Schäfer was a chance discovery. When he directed the beam of a ruby laser through a glass cuvette with fluorescing dye he observed a lasing effect. The reflections of the glass walls were sufficient to react as a resonator. Later, T.W. Hänsch used the dye laser with frequency-selective optical elements for spectroscopy. Today, dye lasers are still in use as cw lasers pumped with argon ion lasers or frequency-doubled Nd:YAG lasers. The advantage of the dye laser is its broad tuning range, up to 100 nm with one dye. Numerous dyes are available, covering the whole range in the visible spectrum. However, low-cost diode lasers have become an interesting alternative, specially for photodynamic therapy.

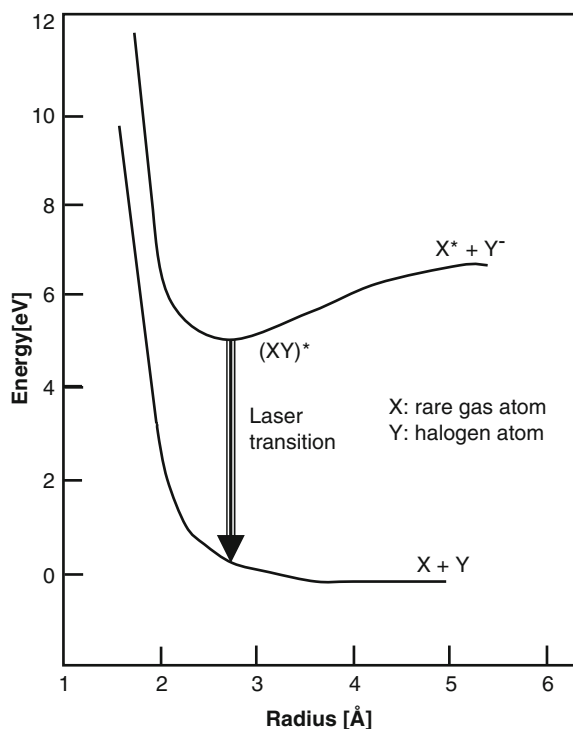


Fig. 1.24 Typical potential curves of rare gas-monohalide excimers

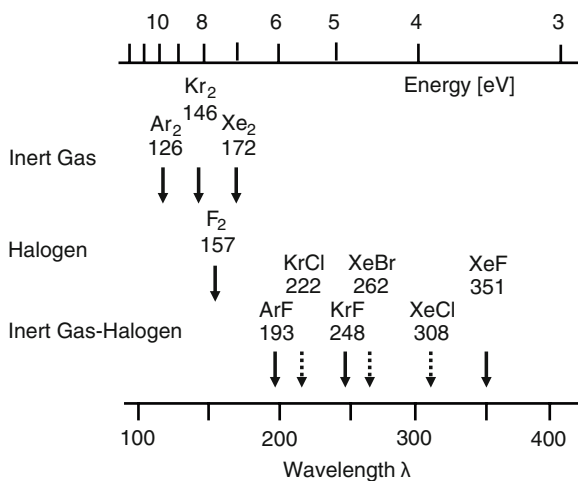


Fig. 1.25 Laser wavelengths of the different excimers in nanometers

Pulsed dye lasers are routinely used in dermatology for treatment of vascular malformations.

Some of the fluorescing dyes used in dye lasers are rhodamine 6G (R6G), fluorescein, coumarin, stilbene, umbelliferone, tetracene, and malachite green [16].

The dye laser is a four-level laser. R6G has been chosen as an example in Fig. 1.26. Photon absorption of the

R6G molecules excites the molecules from the bottom of the S_0 -band to the higher S-bands. All excited states in the higher S-bands contribute to the laser activity because there is a very fast transition (10^{-12} s) of the vibration-rotation energy levels within one S-band to the lowest energy level, where they will have a Boltzmann distribution. Also, transitions from higher S-bands, to the S_1 -band, as demonstrated in Fig. 1.26, are very fast (10^{-11} s) compared to the fluorescence lifetime of $\geq 10^{-8}$ s.

Transitions from S_1 to the vibration-rotational energy levels in the S_0 -band are responsible for the different laser lines that continuously can be tuned within the range of the dye used.

1.6.4 Diode Laser (Semiconductor Laser)

Hall and his team at General Electric were the first to demonstrate the emission of a semiconductor laser diode in 1962 [9].

Laser diodes are formed by doping very thin layers on the surface of a crystal wafer to produce an *n-type* region (negative, increase of negative free charges – electrons) and *p-type* region (positive, increase of free positive charges – holes), one above the other, resulting in a *p-n* junction. Applying a forward electrical bias causes the two species of charge carriers, holes, and electrons, to be injected from both sides of the *p-n* junction into the depletion zone, situated in the centre of the *p-n* junction. Holes are injected from the *p*-doped semiconductor and electrons from the *n*-doped semiconductor (see Fig. 1.27). Recombination or annihilation of both charges results in a spontaneous emission of a photon, with energy equal to the difference between the electron and hole states involved.

The difference between the photon-emitting semiconductor laser and conventional diodes lies in the use of a different type of semiconductor. Photon-emitting semiconductors are the so-called *direct bandgap* semiconductors. These semiconductors are compound semiconductors, in contrast to silicon and germanium, which are single-element semiconductors that do not emit photons. Compound semiconductors have crystalline Structures that are virtually-identical to silicon or germanium but use alternating arrangements of two different atomic species in a checkerboard-like pattern. Such materials are gallium arsenide, indium phosphide, gallium antimonide and gallium nitride.

In the absence of lasing, holes and electrons can coexist in proximity to one another, without recombining,

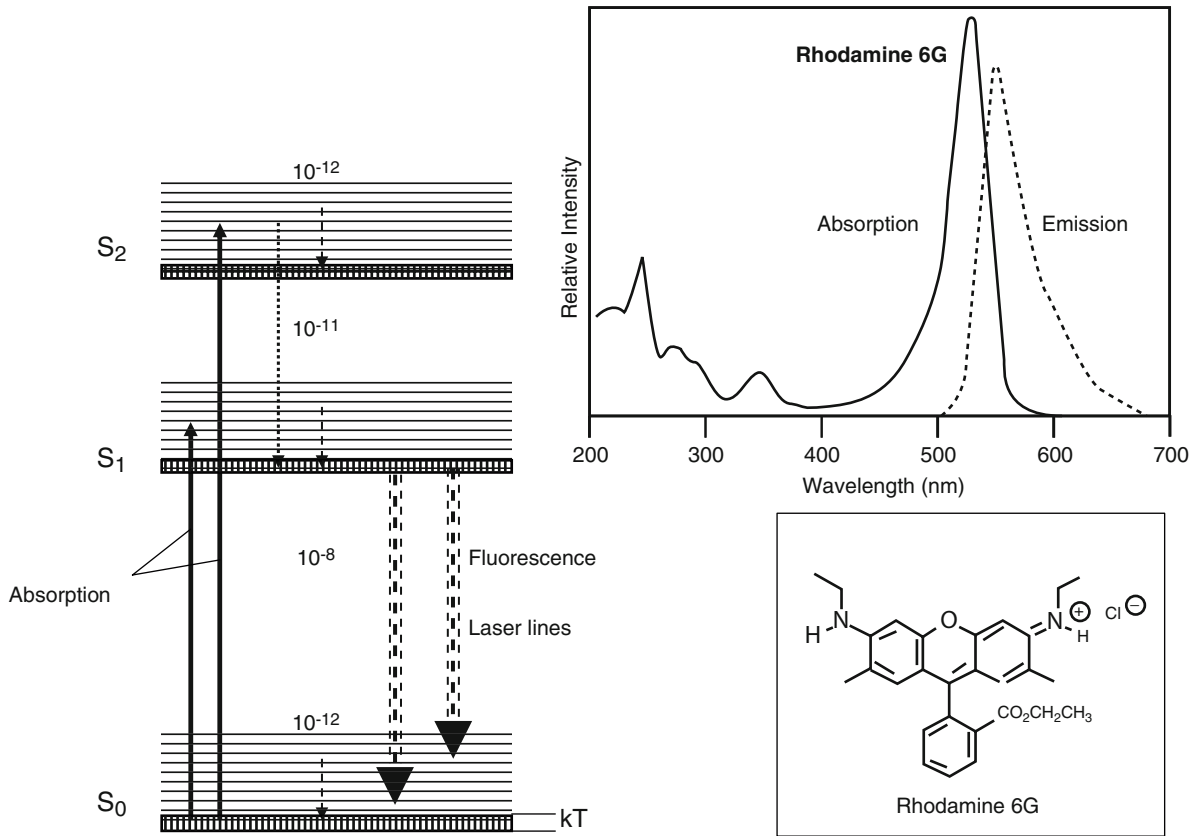


Fig. 1.26 Scheme of a dye laser. Inserts show the structure of rhodamine 6G (bottom) with absorption and emission spectra (top)

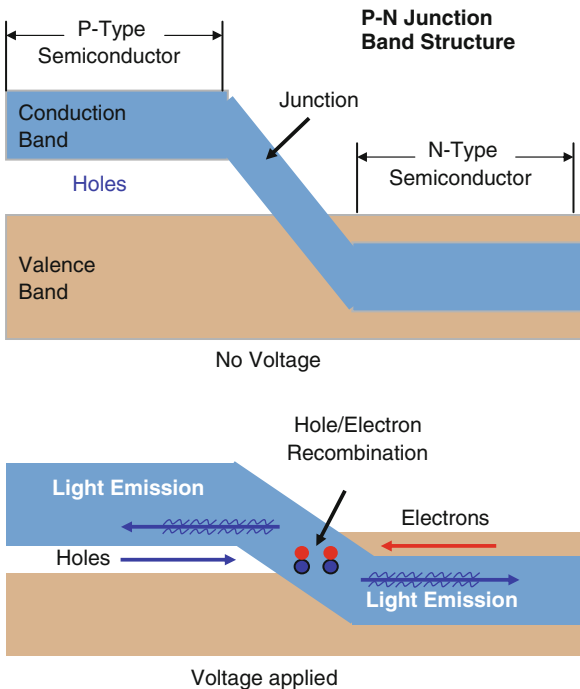


Fig. 1.27 Band gap structure of laser diodes

for a certain time, termed the “upper-state lifetime” or “recombination time,” about a nanosecond, before they recombine. A nearby photon with energy equal to the recombination energy can cause recombination by stimulated emission. This generates another photon of the same frequency, travelling in the same direction, with the same polarisation and phase as the first photon. This stimulating emission causes light amplification in the $p-n$ junction region proportional to the number of electrons and holes being injected.

A simple form of a laser diode consists of an optical waveguide as the optical cavity, made on the crystal surface, such that the light is confined to a relatively narrow line (see Fig. 1.28). When the two ends of the crystal are cleaved to form perfectly smooth, parallel edges, they form a Fabry-Perot resonator. The laser diode will start to lase when the losses (spontaneous emission, absorption, incomplete reflection) are surpassed by the stimulating emission.

Laser diodes are very efficient, with an electrical current to light conversion of up to 60%. Therefore, they are well suited for medical applications because they

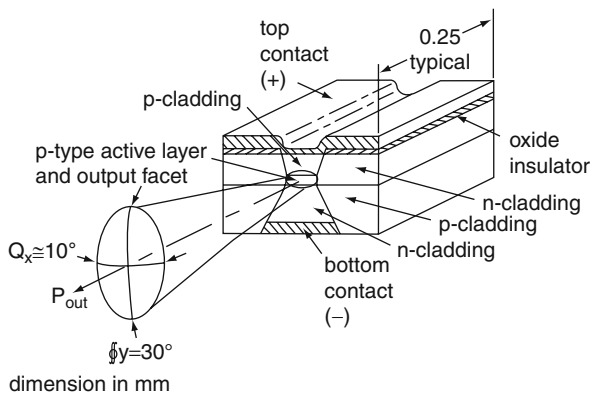


Fig. 1.28 Schematic drawing of a laser diode with asymmetric light emission. Emitting surface is about $1\ \mu\text{m}$ high and $100\ \mu\text{m}$ wide

are very powerful (up to 100 W), they are small devices, and they are flexible in wavelength. Laser diodes are available from the UV spectrum (for chromophore excitation) into the visible spectrum until the near-IR spectrum for surgical applications.

Laser diodes with a single emitter, as demonstrated in Fig. 1.28, may have an optical output of 10 to 40 W. Peltier elements are normally integrated to cool the diodes. Even higher power is obtained by diode bars, where 20–50 single emitters, $100\ \mu\text{m}$ broad, are aligned in one stripe with a fill factor of 50%. Such bars can be mounted one above the other to form a stack of several 100 W output power.

Take Home Pearls

- New developments in laser technology provide higher efficiency in laser light generation and miniaturisation to improve the handling in medical applications.
- Laser light is now available in the range of UV to far IR.
- According to the needs of specific applications, the radiation of laser light can be modulated from cw to femtosecond pulses.
- Experienced dermatologists have now the possibility to select the optimal laser wavelength and pulse regime.

References

1. Basov NG, Danilychev VA, Popov YM. Stimulated emission in the vacuum ultraviolet region. *Sov J Quantum Electron.* 1971;1:18–22.
2. Beaulieu AJ. Transversely excited atmospheric pressure CO_2 lasers. *Appl Phys Lett.* 1970;16:504–5.
3. Demtröder W. *Atoms, molecules and photons.* New York: Springer; 2006.
4. Diels JC, Rudolph W. *Ultrashort laser pulse phenomena.* New York: Academic Press; 2006.
5. Einstein A. Zur Quantentheorie der Strahlung. *Phys Zeitschr.* 1917;18:121–8.
6. Elhilali M, Elzayat EA. Laser prostatic surgery: an update. *Afr J Urol.* 2008;14:1–14.
7. Frank F, Wondrazek F. Erbium:YAG laser. In: Berlien HP, Müller GJ, editors. *Applied laser medicine.* Berlin: Springer; 2003.
8. Gross H. *Handbook of optical systems, vol. 4. (Materials)* New York: Wiley; 2005.
9. Hall RN, Fenner GE, Kingsley JD, Soltys TJ, Carlson RO. Coherent light emission from GaAs junctions. *Phys Rev Lett.* 1962;9:366–9.
10. Hecht J. *Laser pioneers.* New York: Academic Press; 1992.
11. Hoffmann RM. Laser prostatectomy versus transurethral resection for treating benign prostatic obstruction: a systematic review. *J Urol.* 2003;169:210–5.
12. Ivanenko MM, Hering P. Wet bone ablation with mechanically Q-switched high-repetition-rate CO_2 laser. *Appl Phys B.* 1998;67:395–7.
13. Johnson DE. Use of the holmium:YAG laser in urology. *Lasers Surg Med.* 1992;12:353–63.
14. Maiman TH. Stimulated optical radiation in ruby. *Nature.* 1960;187:493–4.
15. Moulton PF. Spectroscopic and laser characterisation of $\text{Ti:Al}_2\text{O}_3$. *J Opt Soc Am B.* 1986;3:125–33.
16. Nair LG. Dye lasers. *Prog Quantum Electron.* 1982;7:153–268.
17. Pearle MS, Drach GW, Roehrborn CG. Safety and efficacy of the alexandrite laser for the treatment of renal and ureteral calculi. *Urology.* 1998;51:33–8.
18. Pollack SA, Chang DB. Ion-pair upconversion pumped laser emission in Er^{3+} ions in YAG, YLF, SrF_2 and CaF_2 crystals. *J Appl Phys.* 1988;64:2885–93.
19. Pollnau M, Jackson SD. Erbium 3- μm fiber lasers. *IEEE J Sel Top Quantum Electron.* 2001;7:30–40.
20. Riehle F. *Frequency standards – basics and applications.* Weinheim: Wiley-VCH; 2004.
21. Saleh BEA, Teich MC. *Fundamentals of photonics.* In: Wiley series in pure and applied optics. New York: Wiley; 2007.
22. Schawlow AL, Townes CH. Infrared and optical masers. *Phys Rev.* 1958;112:1940–9.
23. Temelkuran B, Hart SD, Benoit G, Joannopoulos JD, Fink Y. Wavelength-scalable hollow optical fibers with large photonic bandgaps for CO_2 laser transmission. *Nature.* 2002;420:650–3.
24. Townes CH, Theodore H, Maiman (1927–2007). Maker of the first laser. *Nature.* 2007;447:654.
25. Wendt-Nordahl G, Huckele S, Honeck P, et al. Systematic evaluation of a recent introduced 2- μm continuous-wave thulium laser for vaporessection of the prostate. *J Endourol.* 2008;22:1041–6.

Core Messages

- › Understanding laser-tissue interactions and using the laser in an optimal way are the most important messages in this chapter.
- › The wavelength-dependent penetration depth of laser light into tissue determines heat flow and the thickness of the zone of necrosis.
- › The concept of photothermolysis, introduced by Rox Anderson, improved specificity of laser-tissue interactions.
- › Thermal lasers are used for tissue coagulation and vaporisation.
- › For tissue ablation, high absorption of the laser light by the tissue is necessary, as is high power density of the laser pulse (>100 kW/cm²).
- › Keep in mind that the shorter the laser pulse or the laser irradiation on the same spot, the smaller will be the zone of necrosis.
- › Consider possible acoustic side effects with short and ultrashort laser pulses.

dominates their behaviour. When photons strike the surface of the tissue, because of the refractive index change, a portion (4–10%) of the photons are reflected according to the angle of incidence. Photons penetrating the surface initially are refracted, obeying the law of Snellius, which states that photons entering a medium with a higher refractive index are refracted towards the vertical axis to the surface (Fig. 2.1). The refractive index of tissue (n_{tissue}) is ~ 1.4 . Snellius' law states:

$$\frac{\sin \alpha_1}{\sin \alpha_2} = \frac{n_2}{n_1} = n_{12}.$$

In the tissue, the photons may be scattered, changing their direction of flight according to the probability function expressed as the anisotropy factor, g , or absorbed, exciting the absorbing molecule by an electronic transition.

2.1.1 Absorption

The energy states of molecules are quantized; therefore, absorption of a photon takes place only when its energy, $E=h\nu$, corresponds to the energy difference between such quantized states.

Absorption of a photon by a chromophore causes either a quantized change in the distance between charges (electron transition, ultraviolet or visible spectrum; Fig. 2.2) or a quantized change of vibrational modes of the molecule (vibration transition, near infrared [NIR]; Fig. 2.3).

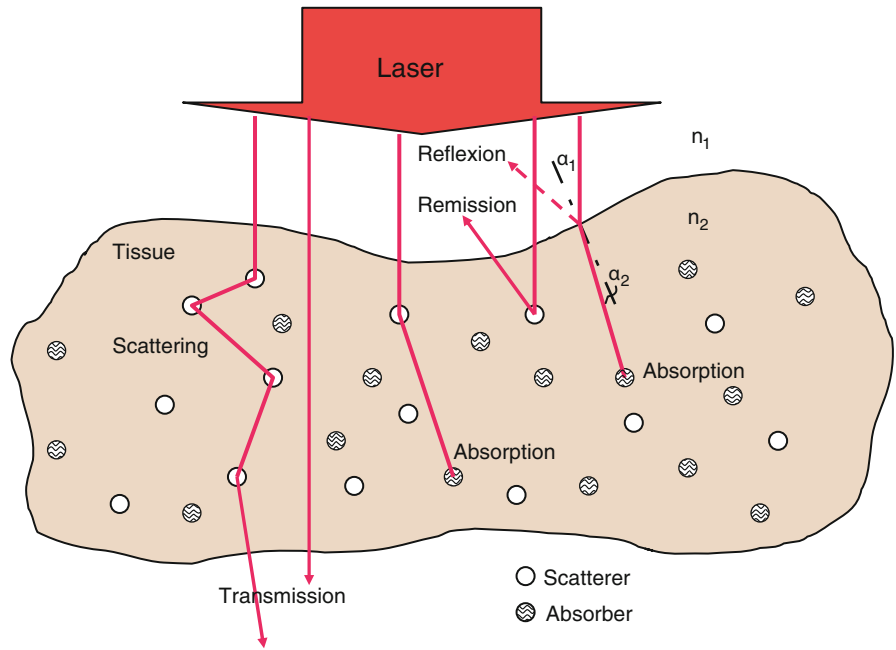
Absorbing molecular components of the tissue are porphyrin, haemoglobin, melanin, flavin, retinol, nuclear acids, deoxyribonucleic acid (DNA)/ribonucleic acid (RNA), and reduced nicotinamide adenine dinucleotide,

2.1 Optical Properties of Tissue

To understand the various modalities of laser-tissue interaction, it is necessary to get an overview of how photons penetrate biological tissue and how physics

R. Steiner
Institut für Lasertechnologien in der Medizin und
Meßtechnik an der Universität Ulm, Helmholtzstraße 12,
89081, Ulm, Germany
e-mail: rudolf.steiner@ilm.uni-ulm.de

Fig. 2.1 Optical behaviour of a tissue layer during irradiation with laser light



Electronic transitions (UV and visible light)

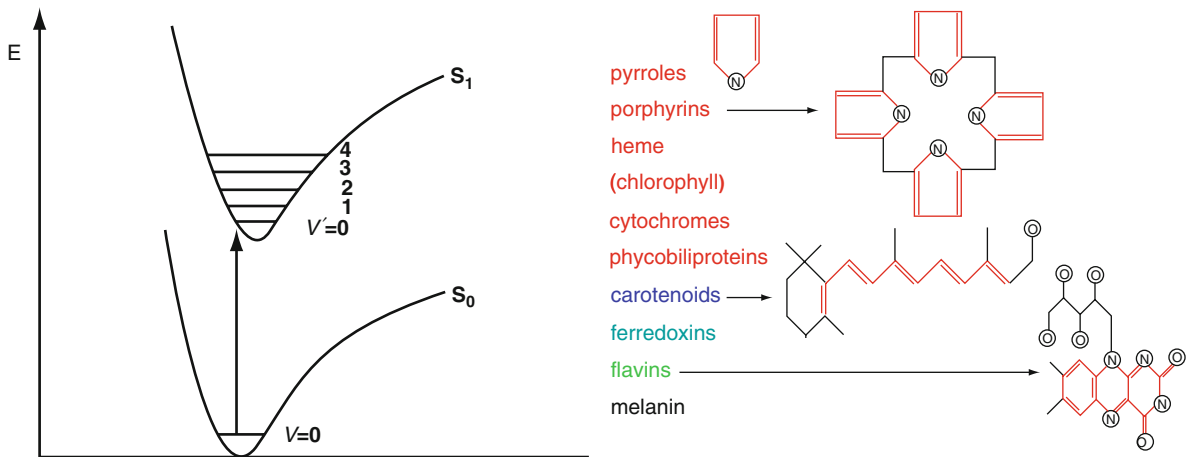


Fig. 2.2 Scheme of electronic excitation after photon absorption and a list of some chromophores in the tissue with the chemical structure. UV ultraviolet

UV ultraviolet

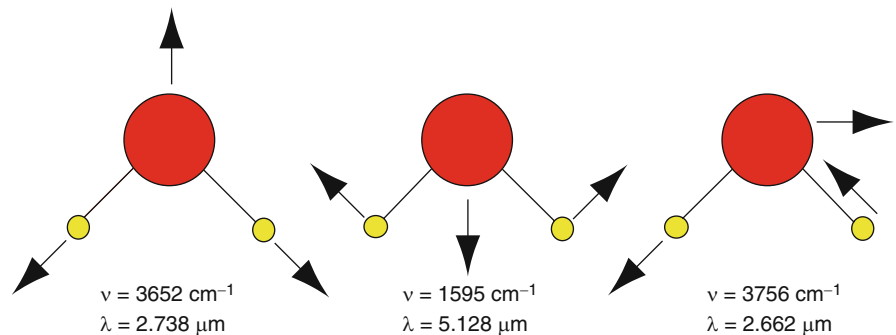


Fig. 2.3 Vibration transitions of a water molecule with its absorption bands

where electronic transitions are excited, leading to discrete and intense (broad) absorption bands. In the NIR and mid-infrared (MIR) region, tissue absorption is dominated by water absorption, with the maximum at 3 μm . The coefficient μ_a (cm^{-1}) characterizes the absorption. The inverse, l_a , defines the penetration depth (mean free path) into the absorbing medium.

To understand the mechanism of absorption, one can imagine a chromophore with a geometrical cross-section of size A (cm^2) being placed in a parallel laser beam (Fig. 2.4). The shadow it creates is the effective cross-section σ_a (cm^2), which in most cases is smaller than the

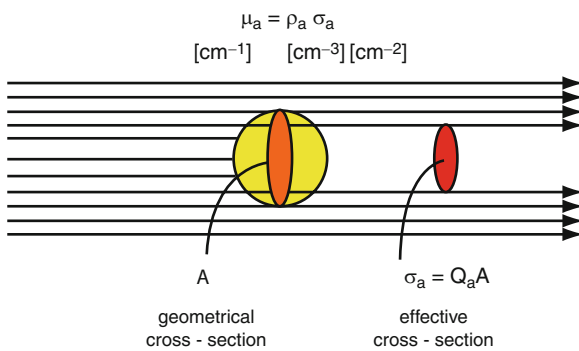


Fig. 2.4 Definition of the absorption coefficient by the cross-section of chromophores and their volume densities

geometrical cross-section A . When there are a lot of chromophores in a solution with volume density ρ_a (cm^{-3}), then the absorption coefficient is $\mu_a = \rho_a \sigma_a$ (cm^{-1}).

Chemists normally use Beer's law when they calculate the transmission of light through a cuvette of a dimension, d , filled with absorbing liquid. Then the expression for the transmission, T , is

$$T = I / I_0 = 10^{-\epsilon cd} = 10^{-\rho}$$

where:

- ϵ : molar extinction coefficient [$\text{L}/\text{mol}\cdot\text{cm}$]
- c : concentration of chromophores [mol/L]
- l : optical path (cm)
- ρ : optical density (OD) or extinction

Physicists, however, describe the transmission, T , as

$$T = I / I_0 = \exp(-\sigma_a N_a l) = \exp(-\mu_a l),$$

where:

- σ_a : effective cross-section of absorption (cm^2)
- N_a : density of the absorbing molecules (cm^{-3})
- l : optical path (cm)
- μ_a : absorption coefficient (cm^{-1})

The absorption spectra of different chromophores of biological tissue and water are plotted in Fig. 2.5.

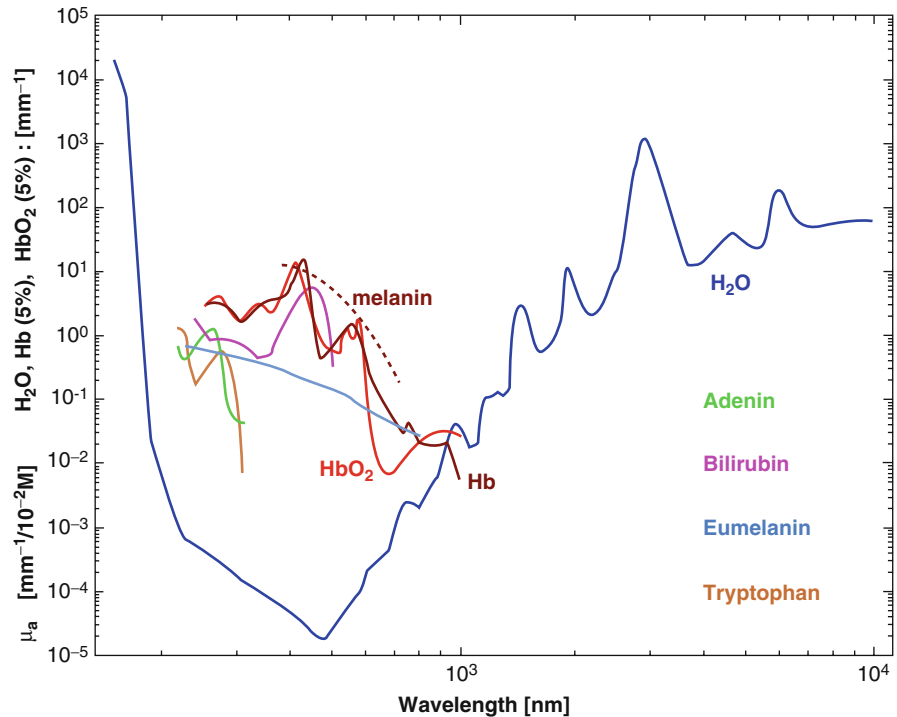


Fig. 2.5 Absorption spectra of chromophores in biological soft tissue

2.1.2 Scattering

The scattering behaviour of biological tissue is also important because it determines the volume distribution of light intensity in the tissue. This is the primary step for tissue interaction, which is followed by absorption and heat generation. Scattering of a photon is accompanied by a change in the propagation direction without loss of energy. Scattering structures of the tissue can be *macroscopic* like muscle fibres, skin layers, or dentin tubules; *microscopic* like cells or intracellular structures; and even *sub-microscopic*, taking into account macromolecules or nanoparticles.

According to the size of the scattering structure, one has to distinguish between Rayleigh scattering, $d \ll \lambda$, and Mie scattering, $d \geq \lambda$. Scattering of tissue is always a combination of Rayleigh and Mie scattering (see Fig. 2.6), depending on what structures are dominant. Rayleigh scattering is rather isotropic, only depending on the polarisation and the wavelength. The scattering cross-section is inverse to λ^4 , which makes the sky “blue.” The equation for Rayleigh scattering is:

$$Q_s = \frac{128\pi^4 a^4}{3\lambda^4} \left| \frac{n_s^2 - n^2}{n_s^2 + 2n^2} \right|^2.$$

Mie scattering, near-field as well as far-field, can be calculated exactly with a Monte Carlo simulation (MCS). Forward scattering is pronounced and is demonstrated in Fig. 2.7, which gives an example of the scattering behaviour of a water droplet of 10 μm in size at a wavelength of 650 nm. Because of the large size of the droplet, one gets interference of scattered light from different locations within the droplet. This results

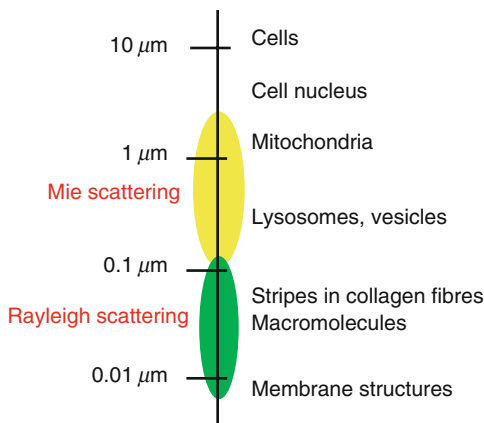


Fig. 2.6 Rayleigh and Mie scattering of tissue structures

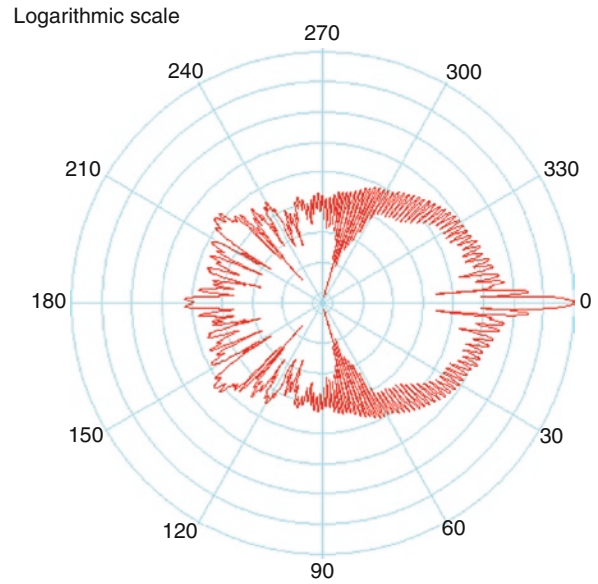


Fig. 2.7 Mie scattering of a water droplet that is 10 μm in size at $\lambda = 650 \text{ nm}$

in intensity maxima when measuring the angle-resolved scattering.

The scattering, similar to absorption, is expressed by the scattering coefficient μ_s (cm^{-1}). The inverse parameter, $1/\mu_s$ (cm), is the mean free path length until a next scattering event occurs. As a rule of thumb, one can say that for red light in the human skin, the mean free path length for absorption is 50 μm , and the mean free path length for scattering is 5 mm. This means that, statistically, a photon is scattered 100 times until it is absorbed.

We have seen from Mie scattering that scattering is not isotropic. Forward scattering is predominant in biological tissue. This characteristic is described by the anisotropy factor g . g can have absolute values from 0 to 1, from isotropic scattering ($g = 0$) to forward scattering ($g = 1$). Negative values for g stand for backward scattering. In tissue, g can vary from 0.8 to 0.99.

Anisotropy factor g : $0 \leq g \leq 1$. $g = 0$: isotropic scattering; $g = 1$: forward scattering.

Taking into account the g value, a reduced scattering coefficient, μ'_s (cm^{-1}), is defined as

$$\mu'_s = \mu_s(1-g).$$

In MCSs, one has to consider a probability function for g in what direction a photon is scattered. The Henyey-Greenstein phase function [7] $p(\theta)$ is often used to describe the angular distribution of light scattered by tissue. It is characterized by the average cosine $\langle \cos \theta \rangle$

of the scattering angle, θ . Since the Henyey-Greenstein phase function is a probability density function, it is normalized to an area of 1 (Fig. 2.9). This model has been applied to numerous situations, ranging from the scattering of light by biological tissue to scattering by interstellar dust clouds. The angular distribution of scattered light is given by

$$p(\theta) = \frac{1}{4\pi} \frac{1-g^2}{(1+g^2-2g\cos(\theta))^{3/2}}.$$

The parameter g characterizes the normalized distribution. For some values of g , Fig. 2.8 shows the probability of scattering from $-180^\circ \leq \theta \leq 180^\circ$. When g approaches the value 1, then the function is very peaked around $\theta=0$. In case of isotropic scattering, $g=0$, there is a constant value of $1/4\pi$ over all scattering angles θ .

The sum of μ_s and μ_a is called the total attenuation coefficient μ_t (cm^{-1}):

$$\mu_t = \mu_s + \mu_a \quad (\text{cm}^{-1}).$$

Measuring the optical constants of biological tissues is not a simple task. In a configuration where a collimated beam hits a tissue sample of defined thickness and only the transmitted photons (ballistic photons) reach the detector, the attenuation coefficient μ_t can be measured.

In general, the optical parameters of tissue like μ_a , μ_s , and g cannot be measured directly. Very complex measuring and evaluation processes are needed to determine such parameters. When a slice of tissue is placed between two integrating spheres (Ulbricht spheres), then the total transmitted and diffusely reemitted radiation can be measured. MCS helps to extract the values of the optical parameters by iteration procedures.

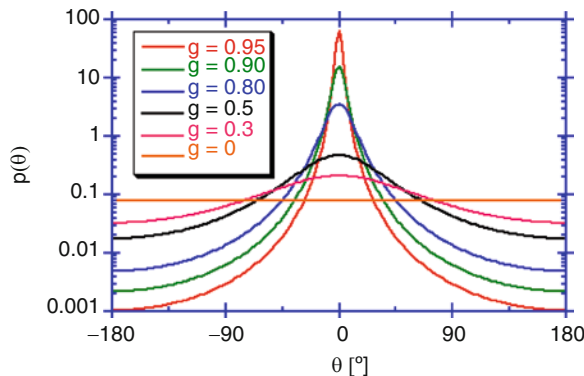


Fig. 2.8 Henyey-Greenstein probability function for different g values

Some other expressions are helpful to describe the optical properties of biological tissue. The fraction of the scattering μ_s over the total attenuation μ_t is called Albedo a :

$$\text{Albedo } a = \mu_s / (\mu_s + \mu_a)$$

Whereas the effective damping coefficient μ_{eff} is defined as:

$$\mu_{\text{eff}} = (3\mu_a(\mu_a + \mu_s'))^{1/2} \quad (\text{cm}^{-1}).$$

The inverse value $1/\mu_{\text{eff}}$, is called the effective penetration depth, d_{eff} , of light into tissue:

$$d_{\text{eff}} = 1/\mu_{\text{eff}} \quad (\text{cm}),$$

and the effective mean free path length, X_{eff} , is as follows:

$$X_{\text{eff}} = 1 / (\mu_a + \mu_s') \quad [\text{cm}].$$

The equation

$$I(d) \propto I_0 e^{-\sqrt{3\mu_a(\mu_a + \mu_s')}d} = I_0 e^{-\mu_{\text{eff}}d}$$

describes approximately the portion of the power of light or photon density, which is transported over a distance d . Photons may propagate undisturbed or may reach the detection surface element after multiple scatterings. If scattering is predominantly in a forward direction, then the transport (reduced) scattering coefficient μ_s' is considerably smaller than μ_s . Single photons arriving at the detector element may have passed a much longer path length (multiple scattering) than distance d .

Photon density penetration into tissue also can be described approximately by the diffusion

$$\frac{\partial}{\partial t} \rho(\vec{r}, t) - D c_m \Delta \rho(\vec{r}, t) + \mu_a c_m \rho(\vec{r}, t) = q_0(\vec{r}, t).$$

With the diffusion constant D ,

$$D = \frac{1}{3(\mu_a + \mu_s')}$$

No analytical solution exists, however, for the transport equation modelling the light penetration into biological tissue. Therefore, in most cases, the MCS [18] has to be used to determine the photon distribution in the tissue. Programmes are available on and can be downloaded free from the Internet. MCS is also useful to model laser-tissue interactions. One example was published by Romero et al. [12].

Table 2.1 A summary of penetration depths in muscle tissue at different laser wavelengths

Wavelength (nm)	Penetration depth ($1/\mu_a$ [μm])	Effective optical penetration ($1/\mu_{\text{eff}}$ [μm])
193	≈ 10	≈ 1
308	50	6
532	830	240
1.064	2.500	1.900
2.060	286	250
2.940	3	3
10.600	17	17

The decision of the appropriate model to calculate the photon distribution and penetration into tissue depends on the values for μ_a and μ_s' [17]. Several cases can be distinguished:

$\mu_a \gg \mu_s'$: Lambert-Beers' law ($\lambda < 300$ nm and $\lambda > 2,000$ nm)

$\mu_a \ll \mu_s'$: the diffusion approximation is valid (650 nm $< \lambda < 1,150$ nm)

$\mu_a \approx \mu_s'$: the transport equation with MCS is valid (300 nm $< \lambda < 650$ nm; $1,150$ nm $< \lambda < 2,000$ nm).

Table 2.1 summarizes the penetration depth in muscle tissue at different laser wavelengths. The mean free path due to absorption and the effective penetration have been considered [3].

It is possible to measure the light distribution inside tissue by introducing a miniaturized probe of 100- μm diameter into the tissue via the hollow needle of a syringe. The measurements confirm the theoretically derived phenomenon that the light intensity directly below the tissue surface is enhanced by a factor of 2–4 as compared with the intensity of the incident beam [15]. The increased fluence rate is caused by scattered photons overlapping with the incident photons. Another observation is that, due to the scattering effect, the penetration depth depends on the irradiated area. Consequently, the penetration depth will double if, for the same irradiance, the beam diameter increases from 1 to 5 mm. For dermatological applications, this effect has to be taken into account. For deep light penetration when treating port wine stains or for hair removal, 10- to 15-mm spot diameters of the laser are recommended.

The measured intensity inside the tissue is called the *fluence rate*. It is the power absorbed by a small sphere divided by the cross-section of the sphere: $A = \pi R^2$.

$$\text{Fluence rate: } F = P/A \text{ (W/cm}^2\text{)}$$

The depth of penetration of laser light into tissue is greatest in the wavelength range of 700–900 nm (optical window). Blood, water, and melanin are the main absorbing components in the tissue (Fig. 2.5). Therefore, Ar⁺ lasers, dye lasers, and diode lasers effectively interact with blood, the Alexandrite laser with melanin, and MIR lasers with the water content of the tissue.

2.2 Reaction Mechanisms

The first systematic presentation of the reaction mechanisms of lasers with tissue was by Boulnois [3] in 1986 (Fig. 2.9). Another important finding was the “selective photothermolysis” (SP) by Anderson and Parish in 1983 [1, 2]. SP is the damage confined to the specific tissue structures by selection of laser wavelength, regulation of pulse duration, and repetition rate.

In the following section we consider the different laser-tissue interaction mechanisms.

2.3 Non thermal, Chemical Reactions

In low-dose irradiation of living tissue, photons may have an influence on the proliferation of cells. Much literature has been published in the past about the interaction of photons (633-nm helium-neon laser or an 820-nm diode laser) with in vitro cell cultures [11] and wound healing by biostimulation. Most of the results, however, were not verified or generated under controlled condition.

2.3.1 Biostimulation

It is well accepted that the energy of photons when absorbed in cells or tissue may affect cellular metabolism and signalling pathways. A review is given by Hawkins-Evans and Abrahamse [6].

Molecular targets can be cytochrome c oxidase (with absorption in the NIR) or photoactive porphyrins. Cellular targets are mitochondria with the effects of increased adenosine triphosphate production, modulation of reactive oxygen species, and initiation of cellular signalling [5], as illustrated in Fig. 2.10.

Fig. 2.9 Plot of laser-tissue interaction mechanisms over time of interaction. Modified from Boulnois JL. Photophysical processes in recent medical laser developments: a review. *Lasers Med Sci.* 1986;1:47–66 [3]

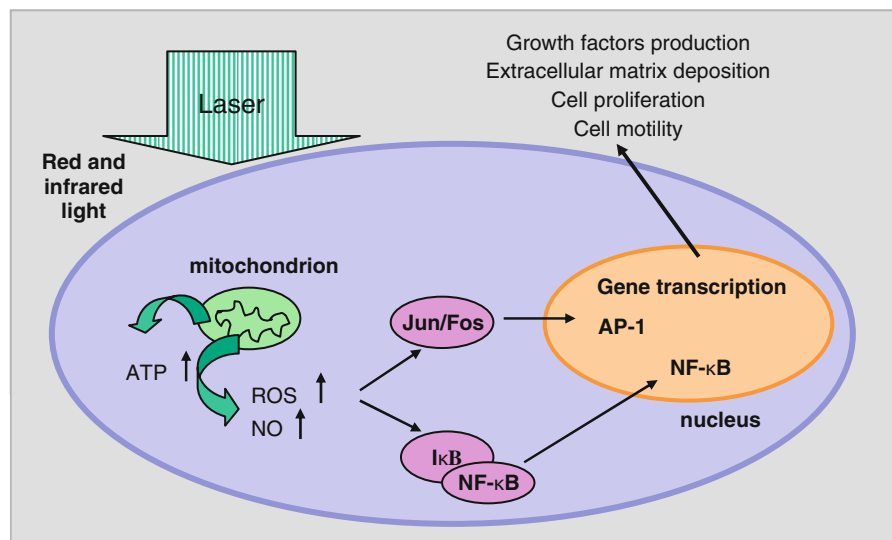
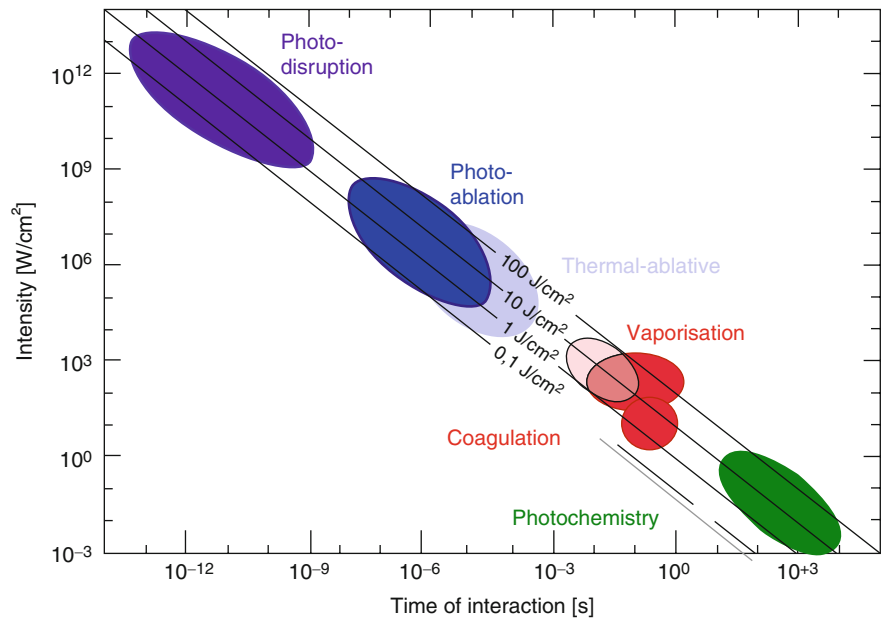


Fig. 2.10 Cell signalling pathways induced by low-level laser therapy. *ATP* adenosine triphosphate, *ROS* reactive oxygen species, *NO* nitric oxide

The results may be:

- Increased cell proliferation and migration (particularly by fibroblasts).
- Modulation in the levels of cytokines, growth factors, and inflammatory mediators.
- Influence on the activity of second messengers (cyclic adenosine monophosphate, Ca^{2+} , nitric oxide).
- Increased tissue oxygenation.
- Increased healing of chronic wounds and improvements in injuries and carpal tunnel syndrome, pain reduction, and impact on nerve injury.

In all cases, the light dose has to be selected carefully because more light is not always better. Spectral regions that show the highest effect of activation are around 633, 690, 820 and 900 nm.

2.3.2 Photodynamic Therapy

Photodynamic therapy (PDT) uses a photochemical reaction with three components: light for activation, sensitizers, and molecular oxygen. The sensitizer molecules

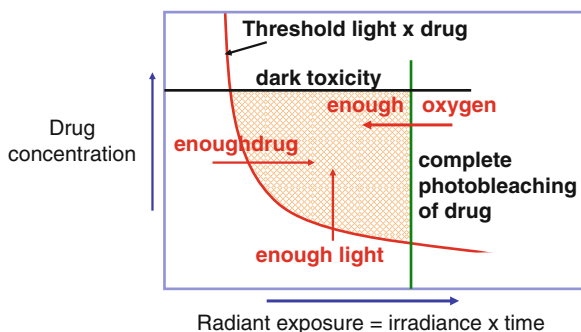


Fig. 2.11 Treatment window for photodynamic therapy

are accumulated in the target cellular structure. They absorb the photons and become excited. After energy transformation from a singlet state to a long-lived triplet state by intersystem crossing, the energy is transferred to oxygen. The excited oxygen (singlet oxygen or radical) destroys the cell. This phototoxic reaction is used in tumour treatment but also in the treatment of precancerous stages or nonmalignant lesions. Sensitizers are also fluorescent. Therefore, they are used for tumour diagnosis and imaging, for example, to visualize bladder tumours in early stages. PDT is described in detail in Chap. 28 of this book.

Here, it is illustrated in the graph of Fig. 2.11 that PDT has a treatment window depending on drug concentration, dark toxicity, radiant exposure of laser light, and sufficient oxygen supply. Therefore, dosimetry is very important for a successful treatment to control all these parameters, especially in deeper layers of the tissue. Sensitizer concentration accumulated in the target tissue and photobleaching during irradiation can be monitored by increase or decrease of the fluorescence intensity.

2.4 Thermal Reactions

The energy of laser irradiation is transferred into heat due to the absorption of the photons by tissue components, DNA/RNA, chromophores, proteins, enzymes, and water. According to the degree of heating, step-wise and selective thermal damage can be achieved:

- 42–45°C: beginning of hyperthermia, conformational changes, and shrinkage of collagen;
- 50°C: reduction of enzymatic activity;
- 60°C: denaturation of proteins, coagulation of the collagens, membrane permeabilisation;

- 100°C: tissue drying and formation of vacuoles;
- >100°C: beginning of vaporization and tissue carbonisation;
- 300–1,000°C: thermoablation of tissue, photoablation and disruption.

The corresponding pathologic analysis of photothermal effects is well described by Thomsen [16]. Examples of coagulation and tissue vaporization are presented in Fig. 2.12.

The laser irradiation that is absorbed by the tissue will heat the tissue, and the temperature increase, ΔT , is given by the absorbed thermal energy per unit volume, Q (J/cm³), divided by the density, ρ (g/cm³), and the specific heat, c_w [J/g°K]:

$$\Delta T = Q / \rho c_w \text{ [°K]}$$

Thermal diffusion is responsible for heat flow into the tissue. If the exposure time with a laser pulse, t_p , is short compared to the diffusion time, t_d , then we have “thermal confinement” and the pulse energy is converted into heat [10, 13, 14] in a tissue volume determined by the inverse absorption coefficient, $1/\mu_a$, and the spot size, d . The diffusion time is

$$t_d = 1 / \kappa \mu_a^2 \text{ [s]}$$

The thermal diffusion coefficient κ (m²/s) is determined by the thermal conductivity, Λ [W/m°K], divided by the density and specific heat:

$$\kappa = \Lambda / \rho c_w \text{ (m}^2\text{/s)}$$

Table 2.2 summarizes the thermal coefficients for different biological tissue materials.

Thermal diffusion and the extent of tissue necrosis are related. With low laser power and long irradiation time, thermal necrosis is large. Shortening the laser application time reduces the time for thermal diffusion, and the zone of necrosis becomes smaller. Minimum thermal necrosis is reached when the irradiation time is equal to the thermal diffusion time or thermal relaxation time. Nevertheless, it will not be smaller than the wavelength-dependent penetration depth of the laser light into the tissue.

Thermal damage of the tissue is described by the Arrhenius rate equation. The consequence of this equation is that the threshold for tissue damage depends on the laser power and the application time. This threshold can be reached with high laser power in a very short time, resulting in a higher temperature, or with low power but long irradiation, where the threshold is reached with lower temperature. Figure 2.13 explains this relation.

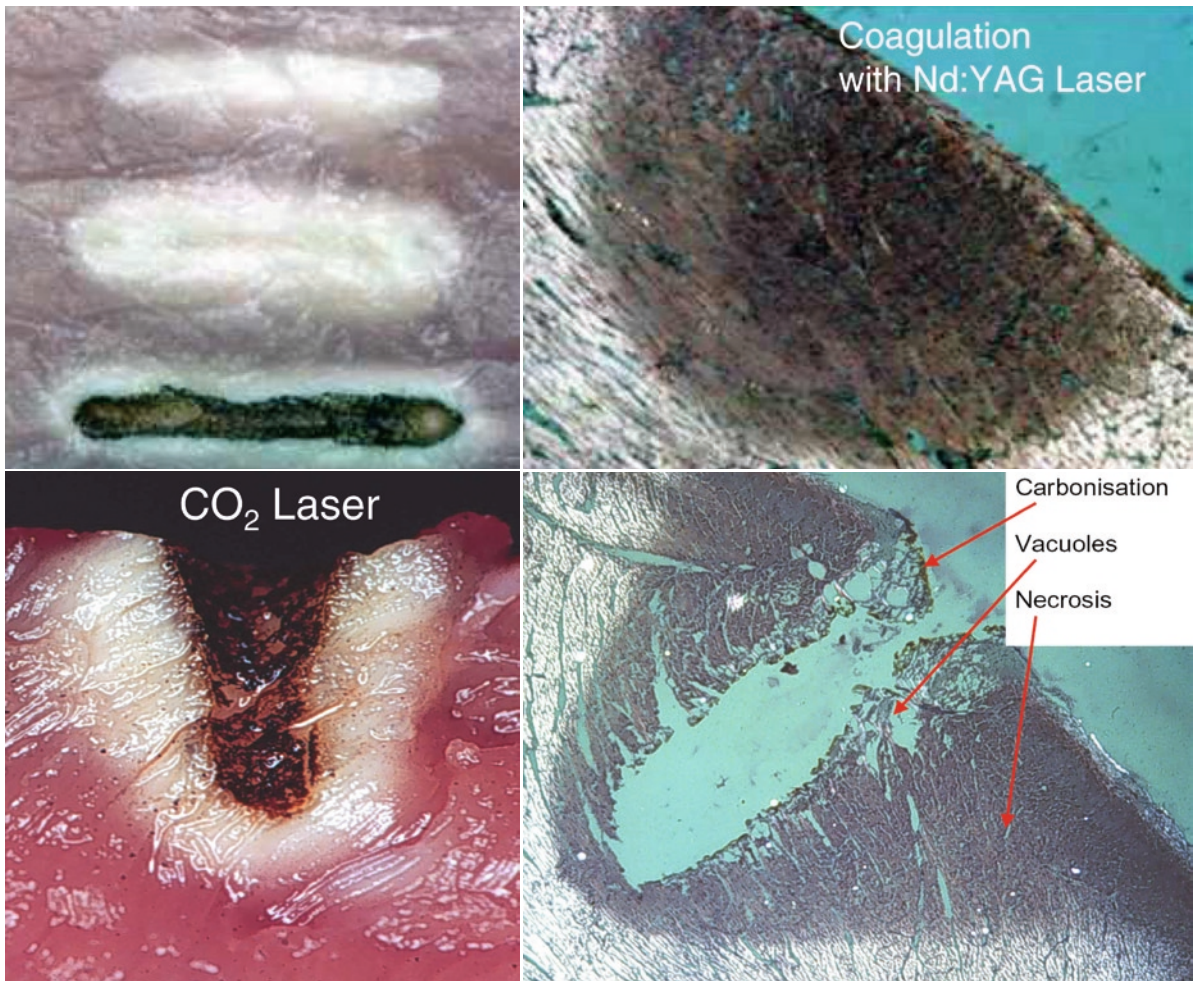


Fig. 2.12 Tissue effects of coagulation and vaporization with corresponding histologies. CO_2 carbon dioxide, $Nd:YAG$, neodymium-doped yttrium aluminium garnet

Table 2.2 Thermal constants for different biological tissues and materials

Material	Density ρ (g/cm ³)	Water content (%)	c_w (J/g K)	Λ (W/m K)
Water	1,000	100	4.183	0.58
Blood	900	55	3.22	0.62
Fat	900	–	1.93	0.3
Cartilage	1,225	60–70	3.06	0.36
Liver	1,200	80	3.42	0.44
Aorta	1,000	80	3.76	0.48
Copper	8,933	–	0.383	384
Diamond	3,510	–	0.502	33,000

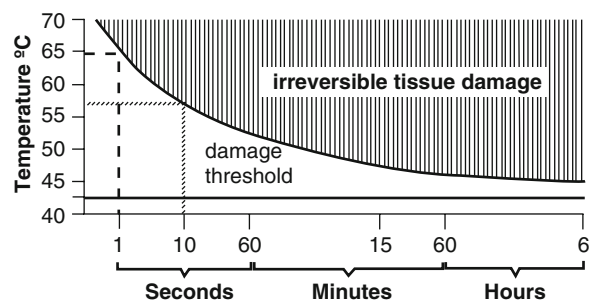


Fig. 2.13 Time-temperature characteristic of tissue damage. The threshold for tissue damage at different temperatures depends on laser power and application time. A 1-s pulse reaches the threshold at 65°C, whereas a 10-s pulse reaches the threshold at 57°C

Example:

The carbon dioxide laser is used in microsurgery for cutting tissue. We want to know the cutting depth by vaporization of the tissue with $p=60$ W, focused to a spot size diameter of 0.4 mm and moved with a velocity of 2 cm/s [4]. Let E_c be the energy for heating the tissue to the boiling point and E_v the latent energy for vaporization per unit volume.

$$E_c = \rho c_w \Delta T [\text{J}],$$

where ρ is the density (here, 1,000 kg/m³ for water), c_w is the specific heat (4,200 J/kg^oK), and ΔT is the difference between the boiling point and body temperature ($\sim 63^\circ\text{K}$).

$$E_v = \rho L_v,$$

where L_v is the latent heat for evaporation (2.3×10^6 J/kg). The evaporated volume per unit time is then

$$V = P / (E_v + E_c) = d \cdot v \cdot d_{\text{cut}}.$$

Hence,

$$d_{\text{cut}} = P / dv (E_v + E_c).$$

With the parameters above for laser power, P , spot size, d and velocity, v , one calculates a cutting depth (d_{cut}) of 3 mm.

This value, of course, is overestimated because we neglected reflection, tissue components other than water, reabsorption by evaporating material, and energy dissipation. Nevertheless, it gives an estimation of the laser reaction on cutting tissue.

2.4.1 Relaxation Time

When the thermal diffusion length, L , is equal to the optical penetration depth, then we have the relation:

$$L = (4\kappa t)^{1/2},$$

where κ is the diffusivity with its value for water of 1.4×10^{-3} cm²/s. When $t = 1$ s, then $L = 0.8$ mm. Taking the optical tissue penetration $1/\mu_a$ as characteristic dimension, we get for the relaxation time:

$$\tau_R = 1/(4\mu_a \kappa).$$

For a carbon dioxide laser, wavelength 10.6 μm , with $\mu_a = 500$ cm⁻¹ and $\kappa = 10^{-3}$ cm²/s, one gets a relaxation time (τ_R) of 1 ms.

2.5 Tissue Ablation

The preconditions for tissue ablation are high absorption and very short laser pulses. Analogous to the *thermal confinement*, one can define a *stress confinement* when tissue is heated up so fast that the pulse duration is shorter than the propagation time, t_m , of the stress wave through the heated volume. The internal stress is described by the *Grüneisen coefficient*, Γ :

$$\Gamma = \alpha / (\rho c_w \kappa_T),$$

where α is the coefficient of thermal expansion, ρ is the density, c_w is the specific heat, and κ_T is the isothermal compressibility. The propagation time, t_m , of the stress wave through the heated tissue volume is

$$t_m = 1 / (c_a \mu_a) [\text{s}],$$

where c_a is the speed of sound in the medium. When the stress wave with velocity c_a cannot leave the heated volume during the laser pulse, then it is removed with the ablation of the material and the surrounding tissue is not damaged.

For the photoablation process, a simple model has been derived to calculate the ablation depth [8, 17]. It is called the “blow-off” model. To ablate tissue, an ablation threshold must be surmounted. The ablation depth, d , per laser pulse is determined by the pulse energy until a saturation threshold. The assumption is that there exists a threshold $F_s(d)$ for the energy density. Below this threshold, no material is removed.

Ablation threshold: $F_s(d) = F_0 \exp(-\mu_a d)$.

The solution for the ablation depth, d , can simply be derived from this expression:

$$d = (1 / \mu_a) \ln (F_0 / F_s).$$

Figure 2.14 explains graphically the threshold behaviour, and Fig. 2.15 gives a demonstration of the ablation process with supersonic particle ejection and the ablated crater in dental hard tissue. Only UV lasers (ArF excimer laser) and pulsed MIR lasers have such high tissue absorption that they are effective ablating lasers.

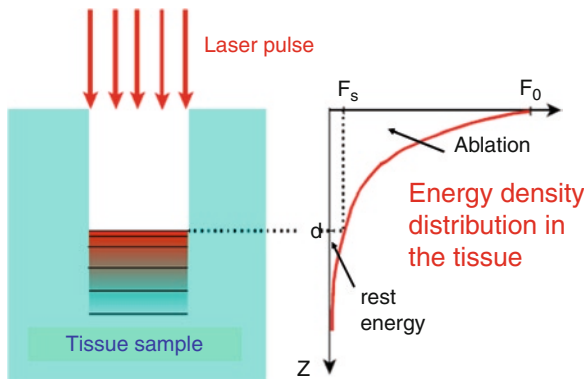


Fig. 2.14 Schematic representation of the blow-off model

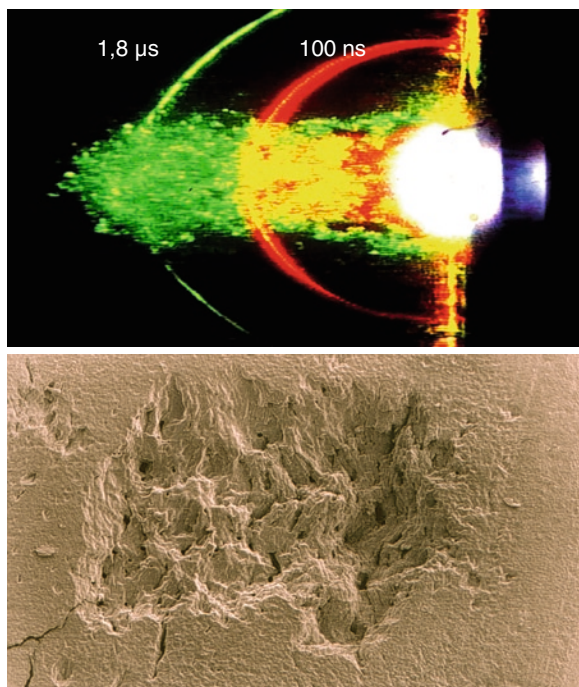


Fig. 2.15 Picture of the ablation process (*top*) and the crater in hard dental material (*bottom*)

The threshold behaviour of highly absorbed laser radiation, e.g., the erbium-doped yttrium aluminium garnet (Er:YAG) laser with a 2,940-nm wavelength, can be used to modulate the thickness of necrosis in soft tissue. Operation of the laser in normal ablation mode does not produce effective thermal necrosis; therefore, no coagulation can stop bleeding. The advantage is that the healing is fast with minimal scarring. However, for precise superficial surgical interventions, it would be helpful if the Er:YAG laser also could coagulate the tissue

and stop bleeding. This is possible by applying between the ablating laser pulses a series of high-frequency sub-threshold laser pulses. The energy of such pulses is below the ablation threshold and therefore is transferred into heat. The heat causes thermal necrosis. The thickness of the necrotic tissue layer can be modulated by the number of sub-threshold pulses. Some Er:YAG laser systems have such operation modes, which are well accepted for microsurgery procedures.

In Fig. 2.16, the addition of the laser pulse heating effect is demonstrated. Certain levels of temperature can be attained, producing thermal necrosis.

A good summary and overview of laser-tissue interaction is the graph in Fig. 2.17. Here, the duration of laser application or duration of laser pulses is plotted for different laser types and their corresponding depth of penetration of biological tissue. Areas are marked for normal thermal reactions, thermal confinement – the pulse duration is shorter than the thermal diffusion length or thermal relaxation time – and stress confinement for ultrashort laser pulses.

2.6 Photodisruption

Focused laser pulses in the nanosecond region (e.g., with a Q-switch neodymium (Nd):YAG laser), or with picosecond or femtosecond durations (titanium (Ti) sapphire laser) develop power densities of 10^{12} W/cm² and more. The electric field strength of this focused radiation is high enough to pull electrons out of the atoms, forming a plasma and producing an optical breakdown with shockwaves disrupting the tissue. The process of this photomechanical reaction is described in detail by Boulnois [3] and Vogel and Venugopalan [17].

Above a light intensity of 10^{11} W/cm², an increased and nonlinear absorption of the light occurs, accompanied by an intense white flash and an acoustic signal – an optical breakdown happens with plasma formation. Multiphoton absorption is responsible for the ionization of atoms. The effect is intensity dependent and scales with I^4 . The free electrons are accelerated in the intense electromagnetic field (inverse Bremsstrahlung), and secondary electrons are produced through collision ionization (Avalanche effect; see Fig. 2.18). The heated electrons and ions form the plasma of 15,000–20,000° K and a pressure of 20–60 bar. It follows

Fig. 2.16 Temperature profiles created by sub-threshold erbium-doped yttrium aluminium garnet laser pulses

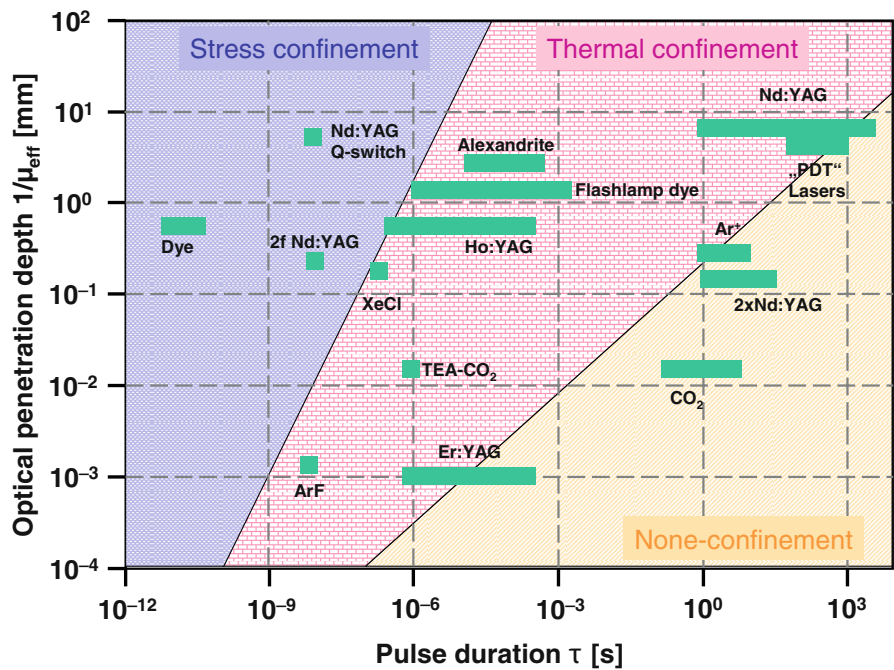
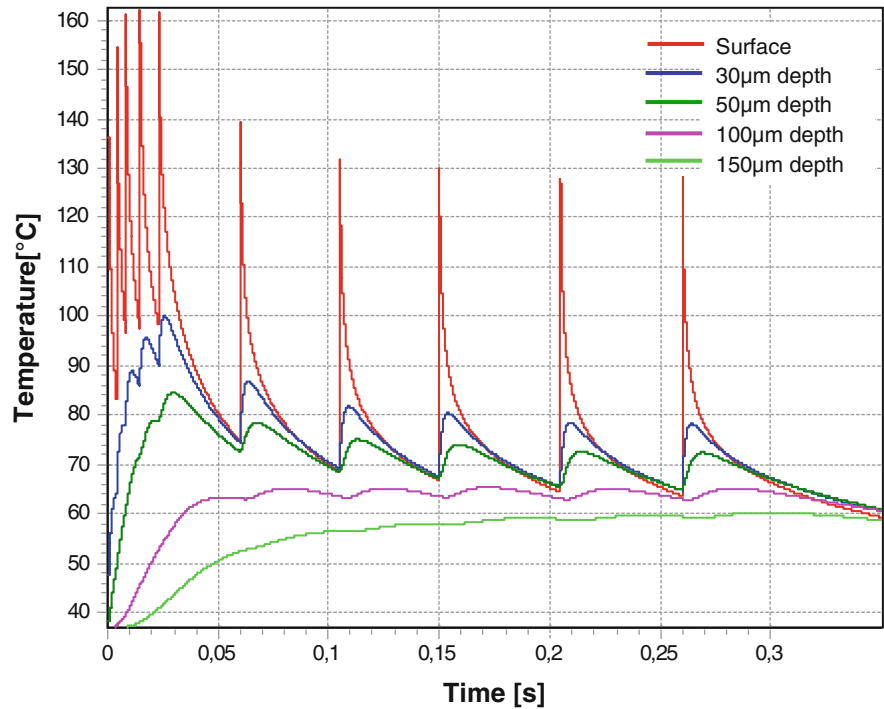


Fig. 2.17 Schematic of laser types, the corresponding tissue reactions, pulse duration, and optical penetration depth

a cavitation bubble of water vapour; the dimension of it depends on the pulse energy and pulse duration. The shorter the pulse, the smaller may be the energy to get an optical breakdown. Hence, the cavitation bubble also will be smaller, and the side effects will be reduced.

The length of the plasma, Z_{max} , created by a focused Gaussian beam, is determined by the Rayleigh length of the focus, Z_R , and the relation of the pulse intensity to the threshold intensity, I_0/I_{th} , for an optical breakdown.

$$\text{Plasma length: } Z_{\text{max}} = Z_R \cdot (I_0/I_{\text{th}} - 1)^{1/2}$$

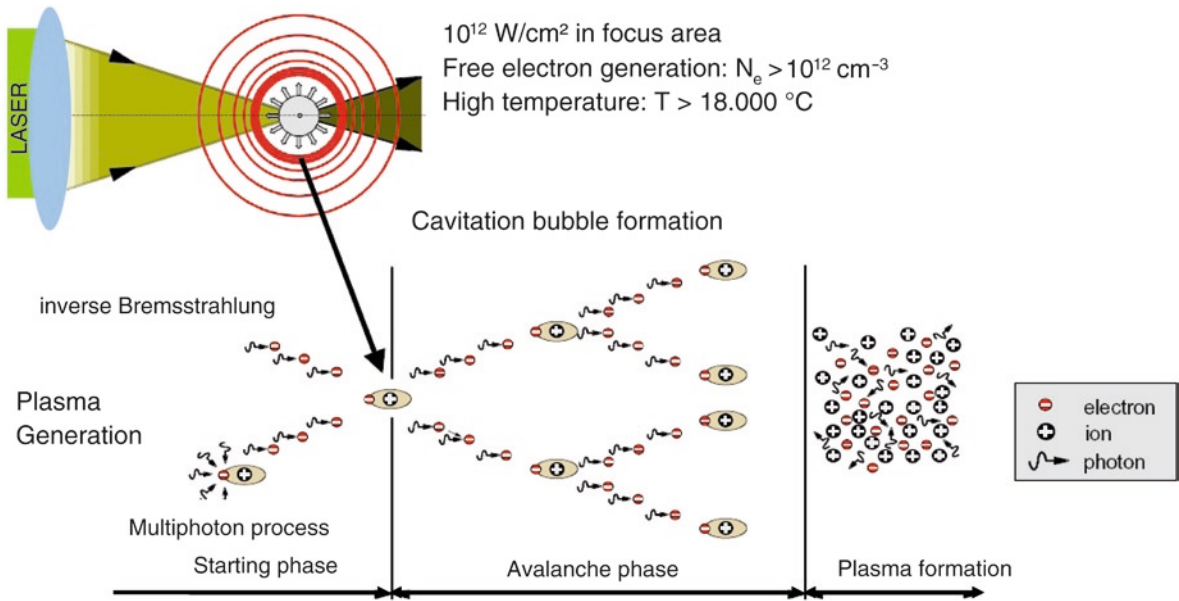


Fig. 2.18 Schematic presentation of the processes responsible for the optical breakdown generated by ultrashort laser pulses

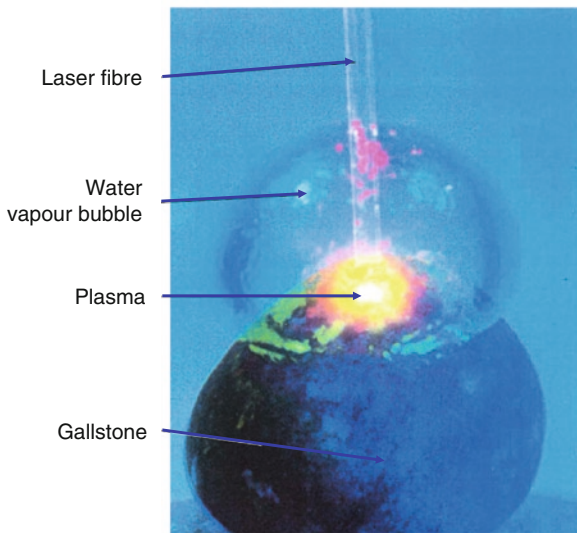


Fig. 2.19 Picture of an optical breakdown with plasma and cavitation bubble [9]

where Z_R is the Rayleigh length, $Z_R = \pi\omega_0^2/\lambda$, with beam waist ω_0 and λ the wavelength in the medium, corrected with the refractive index.

The example of a high-speed camera picture is taken from Ihler [9]. It shows the reaction of a picosecond laser pulse on a gallstone. The laser pulse is guided through a fibre to the stone. The plasma formation and the cavitation bubble are clearly visible.

The bubble has its maximum dimension after about $300 \mu\text{s}$, then it collapses, and normally a multiple rebound effect occurs (Fig. 2.19).

Medical applications of ultrashort laser pulses (100 fs, Ti:sapphire laser) are found in ophthalmology for cutting flaps of the cornea. Soft and hard tissue removal can be done very precisely, but the efficiency is not very high. Therefore, most applications of multiphoton absorption are in microscopy and tissue diagnostics.

Take Home Pearls

- Be sure to use a laser with the right wavelength, power or energy, and pulse regime for your specific application.
- Consider depth of penetration of the light into the tissue and the quadratic power density dependence with the distance (spot size).
- Take the zone of necrosis for blood coagulation into consideration.
- Less laser power is sometimes better to prevent uncontrollable side effects.
- With only one laser device you are limited in your dermatologic applications; do not try to extend it for other applications because you will fail.

References

1. Anderson RR, Parish JA. Selective photothermolysis: precise microsurgery by selective absorption of pulsed radiation. *Science*. 1983;220:524–7.
2. Anderson RR, Margolis RJ, Watanabe S, Flotte T, Hruza GJ, Dover JS. Selective photothermolysis of cutaneous pigmentation by Q-switched Nd:YAG laser pulses at 1064, 532 and 355 nm. *J Invest Dermatol*. 1989;93:28–32.
3. Boulnois JL. Photophysical processes in recent medical laser developments: a review. *Lasers Med Sci*. 1986;1:47–66.
4. Cammarata F, Wautelety M. Medical lasers and laser-tissue interactions. *Phys Educ*. 1999;34:156–61.
5. Gao X, Xing D. Molecular mechanisms of cell proliferation induced by low power laser irradiation. *J Biomed Sci*. 2009;16:4.
6. Hawkins-Evans D, Abrahamse H. A review of laboratory-based methods to investigate second messengers in low-level laser therapy (LLLT). *Med Laser Appl*. 2009;24:201–15.
7. Henyey LG, Greenstein JL. Diffuse radiation in the galaxy. *Astrophys J*. 1941;93:70–83.
8. Hibst R. Technik, Wirkungsweise und medizinische Anwendungen von Holmium- und Erbium-Lasern. In: *Fortschritte der Medizin 15*, Müller, Berlin eds, ecomed verlagsgesellschaft AG & Co.KG, Landsberg; 1997.
9. Ihler B. Laser Lithotripsie-Untersuchung der in-vitro Fragmentierung mit Mikrosekunden-Impulsen, Dissertation Universität Karlsruhe; 1992.
10. Jacques S. The role of tissue optics and pulse duration during high-power laser irradiation. *Appl Opt*. 1993;32:2447–54.
11. Karu TI. Low-power laser therapy. In: Vo-Dinh T, editor. *Biomedical photonics handbook*. London: CRC Press; 2003. p. 48–250.
12. Romero LF, Trelles O, Trelles MA. Real-time simulation for laser-tissue interaction model, *NIC Series* 2006;33:415–422.
13. Steiner R. Thermal and non-thermal laser-dissection. *End Surg*. 1994;2:214–20.
14. Steiner R. Interactions of laser radiation with biological tissue. In: Berlin HP, Müller GJ, editors. *Applied laser medicine*. Berlin: Springer; 2003. p. 101–6.
15. Steiner R, Melnik IS, Kienle A. Light penetration in human skin: in-vivo measurements using isotropic detectors. *SPIE*. 1993;1881:222–30.
16. Thomsen S. Pathologic analysis of photothermal and photo-mechanical effects of laser-tissue interactions. *Photochem Photobiol*. 1991;53:825–35.
17. Vogel A, Venugopalan V. Mechanisms of pulsed laser ablation of biological tissues. *Chem Rev*. 2003;103:577–644.
18. Wang L, Jacques SL, Zheng L. MCML – Monte Carlo modeling of light transport in multi-layered tissues. *Comput Methods Programs Biomed*. 1995;47:131–46.